Research Article

Open Access

M. A. Goudarzi*, M. Cocard, and R. Santerre

Noise behavior in CGPS position time series: the eastern North America case study

Abstract: We analyzed the noise characteristics of 112 continuously operating GPS stations in eastern North America using the Spectral Analysis and the Maximum Likelihood Estimation (MLE) methods. Results of both methods show that the combination of white plus flicker noise is the best model for describing the stochastic part of the position time series. We explored this further using the MLE in the time domain by testing noise models of (a) power-law, (b) white, (c) white plus flicker, (d) white plus random-walk, and (e) white plus flicker plus random-walk. The results show that amplitudes of all noise models are smallest in the north direction and largest in the vertical direction. While amplitudes of white noise model in (c–e) are almost equal across the study area, they are prevailed by the flicker and Random-walk noise for all directions. Assuming flicker noise model increases uncertainties of the estimated velocities by a factor of 5–38 compared to the white noise model.

Keywords: Eastern North America; GPS Time Series; Maximum Likelihood Estimation; Noise Analysis; Spectral Analysis;

1 Introduction

Over the years, velocities of continuously operating GPS (CGPS) stations estimated from their position time series have been widely used for quantifying and explaining the earth's surface deformation. Position time series are, however, are contaminated by both random and time-correlated noise that hinders the accurate estimation of ve-

*Corresponding Author: M. A. Goudarzi: Department of Geomatics Sciences, Louis-Jacques-Casault Building, Laval University, Quebec (QC), G1V 0A6, Canada; Email: mohammad-ali.goudarzi.1@ulaval.ca; Tel: +1 418 656 2530; Fax: +1 418 656 7411
M. Cocard, R. Santerre: Department of Geomatics Sciences, Louis-Jacques-Casault Building, Laval University, Quebec (QC), G1V 0A6, Canada

locities and their uncertainties. Therefore, identifying the noise characteristics in the position time series is a primary challenge. A position time series, however, can be regarded as a signal with deterministic and stochastic parts. Although the deterministic part is nonstationary in nature, it can be well estimated using advanced methods in the time-frequency domain such as S transformation filtering George et al. (2011), and principal component Tiampo et al. (2012). This becomes especially crucial for regions where the signal to noise ratio is small, e.g., intraplate areas affected by the glacial isostatic adjustment (GIA), or for realization of reference frames. The stochastic part is considered as observational noise and can be described by different noise models.

The noise behavior of the position time series should be known a priori or can be estimated from the noise itself to estimate the uncertainties of velocities of a CGPS station reliably. The power-law process Strang and Borre (1997, p. 523) can describe a common statistical model for many types of geophysical signals. The power spectrum P of a stochastic process in a one dimensional time- or space-domain has the form of Williams (2003):

$$P(f) = P_0 \left(f/f_0\right)^{\kappa} \qquad (1)$$

where f is the spatial or temporal frequency, P_0 and f_0 are normalizing constants, and κ is the spectral index Mandelbrot and Van Ness (1968) that can take any real number. However, natural processes are characterized by negative indices due to the fact that they have more power in lower frequencies Kenyeres and Bruyninx (2009). In geophysical phenomena, the spectral index ranges from −3 to +1 Agnew (1992) and is typically divided to the fractional Brownian motion with $-3 < \kappa < -1$, and fractional Gaussian with $-1 < \kappa < +1$ Mandelbrot (1977). Noise processes in the latter interval are stationary or independent of time, while they are nonstationary in the former one. Smaller κ indicates more correlation in time and more relative power for signals with longer periods. Integer spectral indices in this range are of special importance and have specific names: $\kappa = 0$ is equivalent to white noise (WH), $\kappa = -1$ is called flicker noise (FK), and $\kappa = -2$ is named Brownian motion or random-walk noise (RW) Kenyeres and Bruyninx (2009);
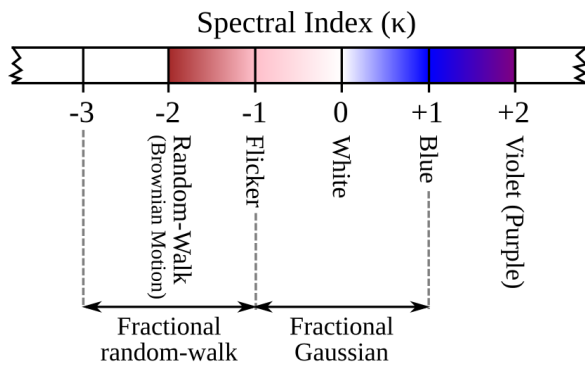
Spectral Index (κ)

Figure 1: Noise spectrum in geophysical phenomena.

Williams (2003). Figure 1 illustrates the noise spectrum and the associated names to the integer values.

The spectral index is a good indicator for characterizing the source of the noise. White noise is generally associated with the GPS hardware noise and measurement errors. It is frequency-independent and contains no or little geophysical information Nistor and Buda (2014). Flicker noise is commonly observed in dynamic processes, e.g., variability of sunspots and the wobble motion of earth about its axis. It is regionally uniform Klos et al. (2014) and can be reduced along with white noise using regional filtering, e.g., common-mode error (CME) filtering described by Wdowinski et al. (1997) by a factor of 2–3 Dong et al. (2006); Williams et al. (2004). Random-walk means that the expected position of the station monument increases as the square-root of time with respect to its initial position Beavan (2005) that indicates a nontectonic motion of the station. The effect of white noise can be reduced by increasing the number of observations and averaging, however, this method is less useful for time-correlated noise and useless for random-walk noise Mao et al. (1999).

There are several evidences for the stochastic part of the CGPS position time series that show measurements are statistically correlated in time rather than simply independent observations Beavan (2005); Lidberg et al. (2010); Mao et al. (1999); Zhang et al. (1997). They show that the uncertainty of velocity estimated by fitting a linear trend to the position time series using the least-squares method is directly affected by the assumed noise model, and discarding the temporal correlation in the data underestimates uncertainty of the estimated velocities by a factor of 5 or more. The temporal correlation is explicitly expressed in the covariance matrix of the data itself Langbein (2008), which is used along with the function to fit the position time series in the least-squares method.

The overall purpose of this paper is to identify the best noise model in the power-law process that can character-

ize the CGPS stations of eastern North America. The analyzed time series are 9 years long on average with up to 14.5 years of data, enabling an accurate assessment of long period time-correlated noise for most of the stations. We used the spectral analysis and the maximum likelihood estimation methods to derive the spectral indices of noise in the position time series and compared the results. As a service to readers, we also study stability of the CGPS stations and identify stations with instable monuments, which are not proper for geodynamic studies. This paper is organized as follows. Section 2 briefly presents the geological setting of the study area where the CGPS stations are located. The details of the selected CGPS stations and their data set are introduced in Section 3. The methods for data processing and analysis are explained in Section 4. The results are then discussed and compared in Section 5. The results of this study are finally summarized in the last section.

2 Region of study

The interior part of the North American tectonic plate is subject to the glacial isostatic adjustment (GIA) and the intraplate tectonic activities. The GIA mainly causes a vertical deformation that affects most of the Canadian landmass in the form of uplift and the northeastern part of the United States in the form of subsidence. Horizontal velocities, as a secondary impact of the GIA, are typically directed radially outward from regions of highest uplift and inward to the regions of maximum subsidence, but have very smaller rates than vertical velocities Henton et al. (2006). Several evidences from geodetic measurements Lambert et al. (2001); Park et al. (2002); Sella et al. (2004) and non-geodetic observations Lavoie et al. (2012) confirm the existence of these phenomena in central and eastern North America. Large earthquakes within the stable plate interiors indicate intraplate seismic activities in this region. Although eastern Canada has a relatively low rate of earthquake activity compared to the west of the country, it is still characterized by many intraplate earthquake patterns from zones with significant earthquakes to zones with very little background seismicity Adams and Basham (1991). This shows vulnerability of the whole region to seismic hazard, particularly in the large urban centers of Quebec City, Montreal and Ottawa.

The earth's surface deformation of eastern Canada has been already studied by some researchers using GPS data. Among them, Mazzotti et al. (2005) studied the seismic region of the Lower Saint Lawrence River valley (SLRV) using observations of 16 GPS stations from the Canadian
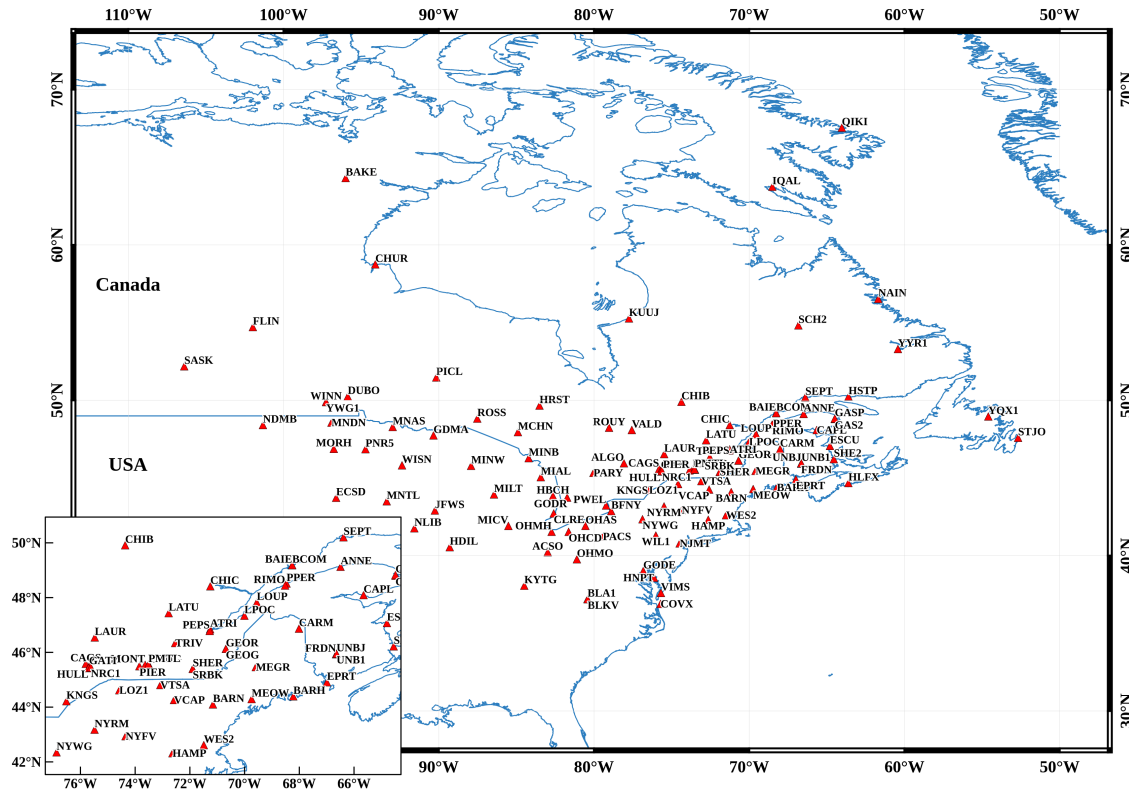
Figure 2: Spatial distribution of the selected CGPS stations. Stations have highest spatial density over the Saint Lawrence River valley, and are shown with a larger scale in the lower-left inset.

base network (CBN). George et al. (2011) have quantified the GIA in eastern Canada using observations of 39 CGPS stations. Williams (2003) constrained the pattern and magnitude of the regional crustal deformation using a subset of 43 CGPS stations. Despite other regions like Southern California and Southern Nevada Langbein (2008); Tiampo et al. (2004); Wdowinski et al. (1997); Zhang et al. (1997), Fennoscandia, and Central Europe Bergstrand et al. (2007); Johansson et al. (2002); Kenyeres and Bruyninx (2009), to the best of our knowledge, there is neither a study about noise behavior of CGPS stations in eastern Canada nor about physical stability of their monuments. This is of special importance because, (a) the intraplate tectonic signal, which is the main cause of deformation has a very low rate, and (b) many CGPS stations are not principally constructed for geodynamic studies, in this region. In other words, no CGPS network has been established in the area with the primary goal of monitoring intraplate tectonic activities like BIFROST network in Fennoscandia Lidberg et al. (2010). Therefore, it is very important to identify instable CGPS stations and exclude them from further studies on deformation such as strain analysis.

3 GPS network and observations

We selected 112 CGPS stations in the study region with more than one year continuous observations. The selected network comprises 25 CGPS stations from the network of the Ministry of Energy and Natural Resources of Quebec (MERN) MERNQ (2014), 32 CGPS stations from the Canadian Active Control System (CACS) NRCan (2014), 46 CGPS stations from the American Continuously Operating Reference Station (CORS) NGS (2014a), 4 CGPS stations from the US National Geodetic Survey (NGS) NGS (2014b), 2 CGPS stations from the Jet Propulsion Laboratory (JPL) JPL (2014), 2 CGPS stations from University of New Brunswick GGE (2014), and 1 CGPS stations from Laval University SCG (2014), listed in Table 1. In this table, 28 stations belong to the International GNSS Service (IGS) Dow et al. (2009) 16 of them designated as reference frame stations, and 7 stations are decommissioned. However, we prefer to keep them because of having long observational period. Figure 2 shows the spatial distribution of the selected CGPS stations.

Table 1: Selected CGPS stations.

Network: *: IGS station, rf: IGS reference frame station, d: decommissioned station.

Monument: DB: Deep-drilled braced, SB: Shallow-drilled braced, CP: Concrete Pillar/Pier, AP: Aluminum Pillar, SP: Steel Pillar, FB: Fixed to building, B: Bedrock, S: Soil/Sand, G: Gravel.

No.	Station	Long. (°W)	Lat. (°N)	Network	Monu.	Start Date	Length (yr)	Epochs (days)	Cleaning steps	Cleaned epochs (%)
1	ACSO	82.981	40.232	CORS	DB	2010.1	4.49	1034	2	0.3
2	ALGO	78.071	45.956	CACS+MERN*^{rf}	CP-B	2000.1	14.49	5176	5	5.0
3	ANNE	66.495	49.128	MERN	FB	2005.1	8.73	2939	3	1.4
4	ATRI	71.262	46.848	MERN	FB	2001.1	13.49	4731	4	1.4
5	BAIE	68.263	49.187	CACS+MERN*	CP-B	2003.3	11.32	4090	4	3.1
6	BAKE	96.002	64.318	CACS*^{rf}	SP-B	2003.3	11.32	3087	2	1.3
7	BARH	68.222	44.395	NGS*^{rf}	FB	2000.1	14.49	4891	2	0.5
8	BARN	71.159	44.099	CORS	SP-S	2001.2	13.39	4018	4	4.5
9	BCOM	68.262	49.187	MERN^{d}	N/A	2001.1	4.51	1552	4	1.5
10	BFNY	78.890	42.878	CORS	FB	2002.7	11.93	3646	3	0.7
11	BLA1	80.420	37.211	CORS	N/A	2006.8	7.84	2080	2	0.1
12	BLKV	80.414	37.206	CORS	CP	2000.1	14.44	3843	2	0.6
13	CAGS	75.807	45.585	CACS*	CP-B	2000.2	14.41	5192	5	6.5
14	CAPL	65.653	48.094	MERN	FB	2002.11	11.63	4120	4	1.4
15	CARM	68.014	46.868	CORS	FB	2004.9	9.82	2630	3	0.9
16	CHIB	74.367	49.913	MERN	FB	2001.1	13.48	4756	5	3.3
17	CHIC	71.255	48.414	MERN	FB	2001.11	12.65	4454	3	1.1
18	CHUR	94.089	58.759	CACS*^{rf}	CP-B	2000.1	14.49	5119	4	2.0
19	CLRE	82.596	42.724	CORS	CP	2003.4	11.22	3551	3	0.9
20	COVX	75.713	36.904	CORS	N/A	2002.1	12.42	3385	3	1.8
21	DUBO	95.866	50.259	CACS*^{rf}	CP-B	2000.1	14.49	5225	3	2.5
22	ECSD	96.614	43.734	CORS	DB	2010.1	4.45	1139	2	0.4
23	EPRT	66.992	44.909	NGS*$^{rf-d}$	CP-B	2002.4	9.75	3036	2	0.7
24	ESCU	64.799	47.073	CACS*	CP-B	2004.12	9.55	3420	3	1.6
25	FLIN	101.978	54.726	CACS*^{rf}	CP-B	2000.1	14.49	5239	4	2.7
26	FRDN	66.660	45.934	CACS*	DB-B	2003.7	11.00	3942	3	2.6
27	GAS2	64.488	48.803	MERN	FB	2011.9	2.77	986	2	0.7
28	GASP	64.487	48.829	MERN^{d}	FB	2008.9	3.01	1040	4	2.3
29	GATI	75.689	45.481	MERN	FB	2009.3	5.33	1920	2	1.6
30	GDMA	90.341	47.748	CORS	FB	2002.5	12.12	3683	3	1.7
31	GEOG	70.687	46.130	MERN	FB	2007.9	6.79	2439	3	1.0

Table 1: ... continued

No.	Station	Long. (°W)	Lat. (°N)	Network	Monu.	Start Date	Length (yr)	Epochs (days)	Cleaning steps	Cleaned epochs (%)
32	GEOR	70.687	46.130	MERN[d]	FB	2003.11	3.83	1329	3	1.5
33	GODE	76.827	39.022	JPL*[rf]	CP	2000.1	14.48	5090	3	1.1
34	GODR	81.728	43.745	CACS	AP	2010.9	1.82	650	2	0.5
35	HAMP	72.639	42.318	CORS	FB	2002.8	11.86	3868	3	1.0
36	HBCH	82.643	43.846	CORS	N/A	2003.4	11.20	3365	2	0.5
37	HDIL	89.294	40.556	CORS	DB	2010.5	4.14	1155	2	1.1
38	HLFX	63.611	44.684	CACS*[rf]	CP-B	2002.12	11.53	4147	3	1.2
39	HNPT	76.130	38.589	NGS*	FB	2000.1	14.49	4956	5	3.2
40	HRST	83.511	49.667	CACS	CP-B	2005.6	8.99	3239	4	2.5
41	HSTP	63.606	50.243	MERN	FB	2001.12	12.53	4141	4	2.0
42	HULL	75.711	45.427	MERN	FB	2001.11	7.32	2493	6	3.5
43	IQAL	68.511	63.756	CACS*	AP-B	2009.9	4.76	1652	4	3.4
44	JFWS	90.248	42.914	CORS	SB	2010.5	4.12	1020	3	0.5
45	KNGS	76.517	44.219	CACS	CP-B	2005.6	8.99	3265	3	0.5
46	KUUJ	77.745	55.278	CACS+MERN*	CP-B	2003.3	11.32	3899	6	4.4
47	KYTG	84.492	38.075	CORS	FB	2008.1	6.41	1851	2	0.9
48	LATU	72.778	47436	MERN	FB	2007.1	7.49	2675	4	1.72
49	LAUR	75.479	46.545	MERN	FB	2004.11	9.65	3441	4	2.2
50	LONG	73.493	45.542	MERN	FB	2008.9	3.34	926	3	1.0
51	LOUP	69.557	47.827	MERN	FB	2005.2	9.40	3336	4	1.5
52	LOZ1	74.583	44.619	CORS	DB (?)	2006.8	6.96	1712	4	1.3
53	LPOC	70.009	47.341	CACS	SP-B	2005.6	9.05	3150	5	3.6
54	MCHN	84.901	47.961	CACS	AP	2009.12	4.49	1575	1	0.0
55	MEGR	69.593	45.464	CORS	CP	2013.3	1.30	474	2	0.4
56	MEOW	69.745	44.296	CORS	FB	2012.8	1.89	680	3	0.7
57	MIAL	83.428	45.063	CORS	FB	2006.7	8.00	1805	2	0.6
58	MICV	85.516	41.923	CORS	CP-S	2006.8	7.83	2384	2	0.3
59	MILT	86.441	43.947	CORS	FB	2005.5	9.16	1857	4	2.8
60	MINB	84.210	46.284	CORS	FB	2007.11	6.65	1470	3	1.1
61	MINW	87.918	45.790	CORS	CP-S	2005.8	8.87	2651	3	1.3
62	MNAS	92.970	48.294	CORS	CP	2010.1	3.84	960	2	1.0
63	MNDN	96.914	48.572	CORS	CP	2010.7	3.98	1261	2	0.7
64	MNTL	93.354	43.508	CORS	CP	2006.4	5.29	946	2	1.8

Table 1: ... continued

No.	Station	Long. (°W)	Lat. (°N)	Network	Monu.	Start Date	Length (yr)	Epochs (days)	Cleaning steps	Cleaned epochs (%)
65	MONT	73.639	45.546	MERN	FB	2001.1	13.49	4676	6	3.0
66	MORH	96.764	46.884	CORS	FB	2009.1	5.45	1455	2	0.8
67	NAIN	61.689	56.537	CACS*^{rf}	CP-B	2003.1	11.49	4152	3	1.5
68	NDMB	101.330	48.416	CORS	FB	2006.6	8.00	2282	3	1.2
69	NJMT	74.483	40.796	CORS	FB	2005.5	9.16	2679	3	0.2
70	NLIB	91.575	41.772	JPL*$^{rf-d}$	CP	2000.1	9.72	3361	3	2.0
71	NRC1	75.624	45.454	CACS*^{rf}	FB	2000.1	14.49	5213	8	6.1
72	NYFV	74.353	42.939	CORS	FB	2006.4	8.18	2571	2	0.4
73	NYRM	75.487	43.178	CORS	FB	2006.4	8.19	2597	2	0.5
74	NYWG	76.876	42.351	CORS	FB	2008.1	5.71	1597	2	0.6
75	OHAS	80.551	41.925	CORS	FB	2006.8	7.87	2430	3	1.2
76	OHCD	81.635	41.541	CORS	FB	2006.1	7.93	2230	2	0.7
77	OHMH	82.731	41.544	CORS	N/A	2004.12	9.04	1701	3	1.1
78	OHMO	81.102	39.777	CORS	FB	2005.11	8.58	2521	2	0.6
79	PACS	79.429	41.239	CORS	FB	2009.4	5.21	1370	2	0.2
80	PARY	80.036	45.339	CACS	AP-B	2005.6	8.99	3256	3	0.6
81	PEPS	71.277	46.785	ULAV	FB	2007.2	6.74	2181	8	4.7
82	PICL	90.162	51.480	CACS*	SP-B	2003.3	11.19	3554	8	5.7
83	PIER	73.848	45.496	MERN	FB	2011.3	3.25	1155	2	0.8
84	PMTL	73.520	45.557	CACS	FB	2008.4	6.20	2184	3	0.6
85	PNR5	94.722	46.863	CORS	FB	2008.7	5.94	1703	3	0.7
86	PPER	68.469	48.517	CACS	CP-B(?)	2008.4	6.17	2176	2	0.8
87	PWEL	79.220	43.237	CACS	AP	2005.6	8.99	3271	3	0.6
88	QIKI	64.034	67.559	CACS*^{rf}	SP-B	2004.7	9.82	3578	4	1.2
89	RIMO	68.521	48.443	MERN	FB	2004.1	9.69	3461	7	3.2
90	ROSS	87.520	48.834	CACS	AP	2005.6	8.99	3267	4	0.7
91	ROUY	79.029	48.241	MERN	FB	2001.1	13.48	4768	4	2.7
92	SASK	106.398	52.196	CACS*	CP-G	2003.5	11.15	4041	4	1.2
93	SCH2	66.833	54.832	CACS+MERN*^{rf}	CP-B	2000.1	14.49	5062	7	5.2
94	SEPT	66.387	50.205	MERN	FB	2005.1	8.68	3005	3	1.1
95	SHE2	64.552	46.221	CACS*	SP-B	2007.2	7.38	2671	4	3.4
96	SHER	71.898	45.401	MERN	FB	2005.4	9.17	3225	2	1.2
97	SRBK	71.898	45.401	MERN^{d}	FB	2001.11	3.47	1197	2	1.3

Continued on next page

Table 1: ... continued

No.	Station	Long. (°W)	Lat. (°N)	Network	Monu.	Start Date	Length (yr)	Epochs (days)	Cleaning steps	Cleaned epochs (%)
98	STJO	52.678	47.595	CACS★^{rf}	CP-B	2000.1	14.49	5174	2	0.8
99	TRIV	72.539	46.344	MERN	FB	2001.11	12.64	4485	5	2.8
100	UNB1	66.642	45.950	UNB^d	FB	2001.7	5.07	1727	3	1.2
101	UNBJ	66.642	45.950	UNB★	FB	2006.8	7.86	2860	3	0.9
102	VALD	77.564	48.097	CACS+MERN★	CP-B	2003.3	11.32	4036	7	4.4
103	VCAP	72.582	44.262	CORS	FB	2000.1	14.49	4690	4	2.6
104	VIMS	75.687	37.608	CORS	FB	2000.1	12.45	3077	2	0.8
105	VTSA	73.083	44.809	CORS	FB	2007.11	6.58	1573	3	1.9
106	WES2	71.493	42.613	NGS★^{rf}	SP	2000.1	14.49	4678	3	2.2
107	WIL1	76.015	41.305	CORS	Tower	2000.1	14.49	4707	3	0.7
108	WINN	97.260	49.901	CACS	FB	2000.1	14.48	5137	4	1.2
109	WISN	92.368	45.822	CORS	CP	2009.1	4.67	1446	2	0.9
110	YQX1	54.598	48.966	CORS	N/A	2008.4	6.18	1758	2	1.0
111	YWG1	97.259	49.901	CORS	N/A	2008.4	6.18	1646	3	0.6
112	YYR1	60.419	53.309	CORS	N/A	2008.4	6.17	1764	2	1.0

Concluded

All of the stations are equipped with dual frequency GPS receivers with geodetic class antenna. There is, however, a great variety of monuments ranging from geodetic-quality concrete pillars anchored to bedrock to non-geodetic stations mounted on top of buildings. We select the data time span of 14.5 years from January 2000 to June 2014, with 4 stations with one to three years, 15 stations with three to five years, 52 stations with five to ten years and 41 stations with more than ten years of observations. The 2000 and later period used here is a convenient one. The complete observation map of all selected CGPS stations is provided in Fig. A.1.

4 Methods and data analysis

4.1 GPS data processing and velocity field

We processed CGPS observations using the automatic processing engine (BPE) of the BERNESE GNSS software (BSW) version 5.0 Dach et al. (2007) on the Regard Laboratory Computer Cluster of our Center for Research in Geomatics (CRG) CRG (2015) along with IGS precise orbits and earth rotation parameters as well as satellites' clock errors. The details of the GPS data processing is the same as in Goudarzi et al. (2015). We aligned the daily network position adjustments to the definition of ITRF 2008 Altamimi et al. (2011) by constraining the position of the following 22 IGS stations to their official values by means of a seven-parameter Helmert transformation: ALGO, BAKE, BARH, CAGS, CHUR, DUBO, EPRT, FLIN, GODE, HLFX, HNPT, KUUJ, NAIN, NLIB, NRC1, PICL, QIKI, SASK, SCH2, STJO, UNB1, and WES2. These stations have relatively longer period of observation with average of more than 12 years with 16 stations designated as the ITRF stations.

The final results are daily earth-centered earth-fixed (ECEF) Cartesian coordinates of stations and their covariance matrices in ITRF 2008. We converted the daily coordinate variations and covariance matrices to the local geodetic (LG) coordinate system using:

$$\Delta \mathbf{x}_i^{(LG)} = \begin{bmatrix} \Delta n \\ \Delta e \\ \Delta u \end{bmatrix}_i^{(LG)} = \mathbf{R}_k \, \Delta \mathbf{x}_i^{(ECEF)} \tag{2}$$

$$= \begin{bmatrix} -\sin\varphi \, \cos\lambda & -\sin\varphi \, \sin\lambda & \cos\varphi \\ -\sin\lambda & \cos\lambda & 0 \\ \cos\varphi \, \cos\lambda & \cos\varphi \, \sin\lambda & \sin\varphi \end{bmatrix}_k \begin{bmatrix} \Delta x \\ \Delta y \\ \Delta z \end{bmatrix}_i^{(ECEF)}$$

and

$$\sum\nolimits_i^{(LG)} = \mathbf{J}_k \sum\nolimits_i^{(ECEF)} \mathbf{J}_k^T \tag{3}$$

$$= \mathbf{R}_k \sum\nolimits_i^{(ECEF)} \mathbf{R}_k^T$$

respectively, where $\Delta \mathbf{x}_i$ is the vector of differential coordinates with respect to the reference epoch and $\sum_i$ is the covariance matrix at epoch i in the corresponding reference system, $\mathbf{R}_k$ is the rotation matrix and $\mathbf{J}_k$ is the Jacobian matrix of the rotation matrix for station k, φ and λ are the geodetic latitude and longitude of station k. Here, we assume the center of the LG coordinates system on the station and take coordinates of each station at epoch $t_0 = 2000.0$ to calculate $\mathbf{R}_k$ and $\Delta \mathbf{x}_i$.

Using the transformed daily coordinates, we formed the position time series and estimated velocities of stations using the following compound model Lidberg et al. (2010); Nikolaidis (2002) implemented in our CGPS time series analysis software called GITSA Goudarzi et al. (2013):

$$\begin{aligned} y(t_i) &= a + b \, t_i \\ &+ c \, \sin(2\pi t_i) + d \, \cos(2\pi t_i) + e \, \sin(4\pi t_i) + f \, \cos(4\pi t_i) \\ &+ \sum_{k=1}^{n_j} j_k \, \mathrm{H}\left(t_i - t_{j_k}\right) + v_i \end{aligned} \tag{4}$$

where t_i for $i = 1, 2, \ldots, N$ are the daily solution epochs in the unit of year, a is the station position, b is the linear velocity, c and d are the annul and e and f are the semi-annual amplitudes of sine and cosine functions. The next term models any number of jump n_j with the magnitude of j_k in the position time series occurred at epoch t_{j_k} (assumed known) using the Heaviside step function $\mathrm{H}(x)$ Abramowitz and Stegun (1972). The last term v_i denotes the measurement errors. Assuming $\mathbf{x} = [a \ b \ c \ d \ e \ f \ \mathbf{j}]^T$ as the vector of unknown parameters, we can rewrite Eq. (4) for all the epochs of a single position time series as:

$$\mathbf{y} = \mathbf{A}\mathbf{x} + \mathbf{v} \tag{5}$$

where $\mathbf{y}$ is the observation vector of daily solutions, $\mathbf{A}$ is the design matrix of observations as:

$$\mathbf{A} = \begin{bmatrix} 1 & t_1 & \sin(2\pi t_1) & \cos(2\pi t_1) & \sin(4\pi t_1) & \cos(4\pi t_1) & \mathrm{H}\left(t_1 - t_{j_1}\right) & \cdots & \mathrm{H}\left(t_1 - t_{j_{n_j}}\right) \\ \vdots & \vdots & \vdots & \vdots & \vdots & \vdots & \vdots & \ddots & \vdots \\ 1 & t_N & \sin(2\pi t_N) & \cos(2\pi t_N) & \sin(4\pi t_N) & \cos(4\pi t_N) & \mathrm{H}\left(t_N - t_{j_1}\right) & \cdots & \mathrm{H}\left(t_N - t_{j_{n_j}}\right) \end{bmatrix}_{N \times (6 + n_j)}$$

and $\mathbf{v}$ is the vector of v_i. The model in Eq. (5) is linear with respect to coefficients and therefore can be solved using the weighted linear least-squares method Mikhail and Ackermann (1976) as:

$$\hat{\mathbf{x}} = \left(\mathbf{A}^T \mathbf{C_y^{-1}} \mathbf{A}\right)^{-1} \mathbf{A}^T \mathbf{C_y^{-1}} \, \mathbf{y} \tag{6}$$

$$\mathbf{C_{\hat{x}}} = \left(\mathbf{A}^T \mathbf{C_y^{-1}} \mathbf{A}\right)^{-1}$$

$$\mathbf{Q_{\hat{x}}} = \hat{\sigma}_0^{-2} \cdot \mathbf{C_{\hat{x}}}$$

$$\hat{\mathbf{v}} = \mathbf{y} - \mathbf{A}\hat{\mathbf{x}}$$

where $\hat{\mathbf{x}}$ is the vector of estimated parameters and $\mathbf{C_y}$ is the covariance matrix of the observations. $\mathbf{C_{\hat{x}}}$ and $\mathbf{Q_{\hat{x}}}$ are the covariance and cofactor matrices of estimated parameters, respectively, and $\hat{\sigma}_0$ is the reference variance. $\hat{\mathbf{v}}$ is the vector of postfit residuals. It should be emphasized that this method can be used when the design matrix $\mathbf{A}$ is deterministic. In the case of a random design matrix, the total least-squares method Fang (2013); Schaffrin and Wieser (2008) provides more accurate estimations. Equation (5) may also be solved using the QR method Rice (2006, p. 593) that avoids rounding error, which tends to increase in Eq. (6).

We identified outliers using median and interquartile range (IQR) statistics Lidberg et al. (2010) that describe the central value and spread of the data with the following condition Nikolaidis (2002):

$$\left| \hat{v}_i - \text{median}\left(\hat{\mathbf{v}}_{i-w/2}, \hat{\mathbf{v}}_{i+w/2}\right) \right| > n \times \text{IQR}\left(\hat{\mathbf{v}}_{i-w/2}, \hat{\mathbf{v}}_{i+w/2}\right) \tag{7}$$

where the median and the IQR functions are applied on the obtained postfit residuals within the window size of w, and n is an integer factor for setting the level of rejection. We set the window length of one year equals to the longest signal period in Eq. (4). A value of n equals to 3 was used for outlier detection Beavan (2005). In this way, maximum 6.5% of data (for station CAGS) was removed after several iterations. The number of cleaning steps and percentage of cleaned epochs are presented in Table 1. The output of this section is the linear velocity of stations and their uncertainties along with the postfit residuals, which will be used for the noise analysis.

4.2 Estimating spectral indices

We estimated spectral indices of postfit residuals using the methods of spectral analysis in the frequency domain and maximum likelihood estimation (MLE) in the time domain in order to study the effect of temporal correlation in the CGPS position time series. In principle, it is possible to fit the power-law function given in Eq. (1) to a periodogram obtained by a Fast Fourier Transformation (FFT) and estimate P_0 and κ. FFT-based methods require evenly-spaced time series, but CGPS position time series are generally subject to gaps due either to the receiver malfunctioning or outlier removal. Using interpolation methods introduces several artifacts to the data in both time and frequency domains, especially when the gap is large Press et al. (1992). Therefore, we use the Lomb-Scargle algorithm to calculate the periodogram of postfit residuals per station per position direction Scargle (1989, 1982, 1981); Schulz and Stattegger (1997). The method has the advantage of evaluating the data of the time series only at measured epochs as well as quantitative significance testing of the results. The normalized Lomb-Scargle periodogram P of a time series $y(t_i)$ for $i = 1, 2, \ldots, N$ is estimated by Mao et al. (1999); Trauth (2010, p. 136):

$$P(2\pi f) = \frac{1}{2\sigma^2} \left(\frac{\left[\sum_{i=1}^{N} (y_i - \bar{y}) \cos 2\pi f (t_i - \tau)\right]^2}{\sum_{i=1}^{N} \cos^2 2\pi f (t_i - \tau)} + \frac{\left[\sum_{i=1}^{N} (y_i - \bar{y}) \sin 2\pi f (t_i - \tau)\right]^2}{\sum_{i=1}^{N} \sin^2 2\pi f (t_i - \tau)} \right) \tag{8}$$

where $\bar{y}$ and σ^2 are arithmetic mean and variance of the data in the time series, respectively, and $2\pi f > 0$. The constant τ corresponds to the time lag that makes the periodogram independent of shifting t_i's by any constant amount, and is defined as Zhang et al. (1997):

$$\tan(4\pi f \tau) = \frac{\sum_{i=1}^{N} \sin 4\pi f\, t_i}{\sum_{i=1}^{N} \cos 4\pi f\, t_i} \tag{9}$$

The periodogram is calculated in the range of the Nyquist frequency, and the resolution of the frequency axis depends on the over-sampling parameter. Then, the power of noise is plotted in dB using logarithm function of base 10 as:

$$P(f) = 10 \times \log_{10}\left(P_v/f_s\right) \tag{10}$$

where P_v is the power spectrum of the postfit residuals estimated from Eq. (8) and f_s is the sampling frequency with the unit of day^{-1}. Then, the spectral index of a power-law process can be estimated in the log-log space using Nikolaidis (2002):

$$\kappa = \frac{P(f)}{10 \times \log_{10}(f)} \tag{11}$$

In practice, especially when the time series is long enough, the spectral index is estimated by fitting a straight line only to the data within the range of frequencies where the power spectra are well approximated Zhang et al. (1997). This prevents the predominance of white noise at high frequencies and decreases the impact of outliers at lower frequencies. For short time series, however, it is preferred to use the whole length of spectra and estimate the spectral indices directly from Eq. (1) using a non-linear least-squares method, e.g., explained by Mao et al. (1999).

The best noise model in the MLE method is the one that maximizes its probability function Teferle et al. (2008) by adjusting the covariance matrix of the data as:

$$\ln\left[\mathrm{lik}\left(\hat{\mathbf{v}}, \mathbf{C}\right)\right] = \frac{-1}{2}\left[\ln\left(\det \mathbf{C}\right) + \hat{\mathbf{v}}^T \mathbf{C}^{-1} \hat{\mathbf{v}} + N\ln\left(2\pi\right)\right] \tag{12}$$

where ln is the natural logarithm function, lik is the likelihood function, det is the determinant of the matrix, $\mathbf{C}$ is the fully populated data covariance matrix that directly impacts uncertainties of the estimated parameters in Eq. (6), N is number of epochs in the position time series, and $\hat{\mathbf{v}}$ is the same as in Eq. (6). Matrix $\mathbf{C}$ can represent different forms of Gaussian stochastic noise Williams et al. (2004), e.g., white, power-law, first-order Gauss Markov or their multitude of combinations. In this research, $\mathbf{C}$ is taken as combination of white and power-law noise with amplitudes of a_w and $b_{\kappa \neq 0}$, respectively:

$$\mathbf{C} = a_w^2 \mathbf{I} + b_\kappa^2 \mathbf{J}_\kappa \tag{13}$$

where $\mathbf{I}$ is the identity matrix and $\mathbf{J}_\kappa$ is the covariance matrix for the appropriate colored noise model, both of them have a size of $N \times N$. The identity matrix resembles the time-invariant of the noise process, while $\mathbf{J}_\kappa$ is the time-dependent covariance matrix of the power-law noise. Williams (2003) explains that the covariance matrix for power-law noise with any spectral index $-3 < \kappa < 1$ can be obtained by a method described by Johnson and Wyatt (1994) using a transformation matrix described by Hosking (1981). Flicker and random-walk noise are special cases of the power-law noise process with $\kappa = -1$ and -2, respectively. For flicker noise, Zhang et al. (1997) have approximated the covariance matrix $\mathbf{J}_{-1}$ as:

$$j_{kl} = \begin{cases} \left(\frac{3}{4}\right)^2 \times 2, & t_k = t_l \\ \left(\frac{3}{4}\right)^2 \times \left(2 - \frac{\log|t_k - t_l|/\log 2 + 2}{12}\right), & t_k \neq t_l \end{cases} \tag{14}$$

for most space geodetic time series ($|t_k - t_l| \ll 2^{22}$). This also defines the scale of flicker noise. For random-walk noise, the covariance matrix $\mathbf{J}_{-2}$ can be expressed as Johnson and Wyatt (1994); Mao et al. (1999):

$$\mathbf{J}_{-2} = \begin{bmatrix} \Delta t_1 & \Delta t_1 & \cdots & \Delta t_1 \\ \Delta t_1 & \Delta t_2 & \cdots & \Delta t_2 \\ \vdots & \vdots & \ddots & \vdots \\ \Delta t_1 & \Delta t_2 & \cdots & \Delta t_N \end{bmatrix}_{N \times N} \quad (15)$$

where $\Delta t_i = t_i - t_0$.

The spectral analysis is generally much faster than the MLE and can be used to quickly determine the predominant noise in the position time series or to test the results of the MLE as an independent source. Nevertheless, it has the following disadvantages: (a) the number of noise models that can be examined using this method is limited Williams (2008), and (b) spectral indices are not necessarily estimated accurately Beran (1994); Mao et al. (1999); Zhang et al. (1997). Some researchers such as Langbein and Johnson (1997); Zhang et al. (1997) and Mao et al. (1999) have used both the spectral analysis and the MLE methods. However, Langbein (2004) and Williams et al. (2004) prefer to use the MLE primarily because, (a) it can simultaneously estimate the noise structure together with the parameters of a time-dependent model of the data, (b) it does not require evenly spaced data, and (c) estimates spectral indices with less bias compared to power spectral methods. In contrast, the MLE has the disadvantage of being computationally time consuming Langbein (2004). In this research, we employed both methods: the spectral analysis to estimate the spectral index of noise, and the MLE to characterize the amplitudes of different noise models in the stochastic part of the position series with integer spectral indices.

5 Results and discussion

5.1 Spectral indices

We estimated spectral indices of the power-law noise from postfit residuals after removing linear, annual, and semi-annual signals as well as probable jumps in the position time series using Eq. (4) and cleaning outliers using Eq. (7). Thus, estimated indices in both methods are based on identical position time series and editing results.

5.1.1 Spectral analysis

We estimated the power spectra of postfit residuals using Eq. (8) for three position directions of each individual station with our GITSA software Goudarzi et al. (2013). Figure 3 shows a typical example of the estimated power spectra for station SCH2 with more than 14 years of data. In this figure, the noise power is nearly constant for up to ~10 days (the crossover period) and increases for longer periods afterward. This implies predominance of temporally uncorrelated or white noise to the right at high frequencies and temporally correlated or colored noise to the left for low frequencies. The high variation in the power spectra for longer periods is due to small number of epochs or the short length of position time series, which is not sufficiently long to be estimated reliably. The frequency that this variation starts at is higher for shorter time series (e.g., GAS2, GODR, and MEGR) and lower for longer time series (e.g., ALGO, ATRI, BLKV, and CAGS). The figure also shows that even though the power of colored noise is underestimated at lower frequencies as a result of removing the linear trend and seasonal variations, in general, it is still higher than the power of white noise Langbein and Johnson (1997). This is critical since it highly affects the estimated slope of the power spectrum or the spectral index. The colored noise would be stronger in presence of linear and seasonal terms Kenyeres and Bruyninx (2009). Capturing the lowest-frequency part of the spectrum is difficult in this method Nistor and Buda (2014) and explains the positive spectral indices in Table 2.

The spectral index is the slope of the best fitted line in a least-squares sense to the power spectrum data. However, the estimation process is very sensitive to the selected frequency band especially at higher frequencies where there are far more data to weight the linear regression compared with the lower frequencies. To avoid biasing the estimated indices, we selected data points with frequencies smaller than $1/15$ day^{-1}. The reason for this choice is the predominance of white noise at high frequencies and a surge of power at the period of ~2 weeks for all the time series. Other surges of power at the periods of ~1 year, ~6 months, and ~9 days are also observed in almost all power spectra. This phenomenon is due primarily to the under-sampling residual semi-diurnal and diurnal crustal tide signatures that causes aliased periodic signals with respect to the discrete 24 hour GPS solution strategy, and secondarily to the longer repeat period of the satellite orbits than the Nyquist period of the semi-diurnal and diurnal tidal signatures, as explained by Penna and Stewart (2003). Figure 4A represents histogram of the estimated spectral indices while their numerical values and uncer-
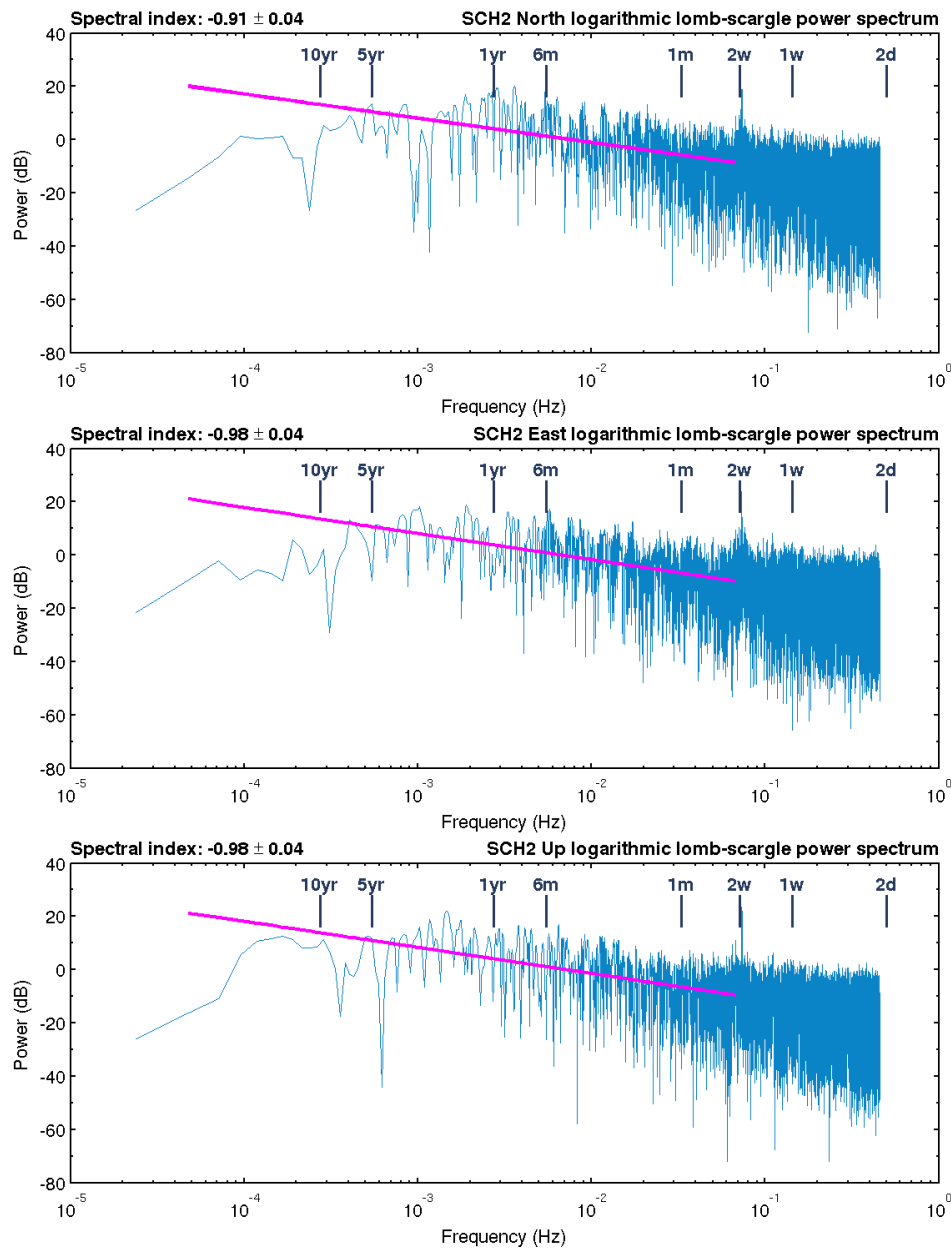
Figure 3: The Lomb-Scargle periodogram and the estimated spectral indices for station SCH2.

tainties can be found in Table 2. Estimated uncertainties are formal standard errors obtained from the linear regression and therefore are optimistic. Spectral indices range between −1.12 and 0.58 for the north, −1.25 and 0.11 for the east, and −0.98 and 0.36 for the up direction. Their weighted means are −0.66 for the north, −0.64 for the east, and −0.55 for the up direction, indicating no significant difference in the spectral character of the noise among individual directions. They are equivalent to the fractional Gaussian part of the noise spectrum and indicate predominance of white plus flicker noise in the position time series.

The weighted mean for all direction is −0.62. Furthermore, histogram of spectral indices shows the highest frequencies at −0.75 for the north and the east directions, while it is shifted to −0.50 for the up direction demonstrating that the flicker noise is stronger in the north and the east directions compared to the up direction.

All power spectra were stacked to estimate a common power index for all stations. The resulted spectrum was then smoothed by a moving average filter with different window lengths of 7, 11, and 21 days. Figure A.2 shows the resulted spectrum for the window length of 11 days.
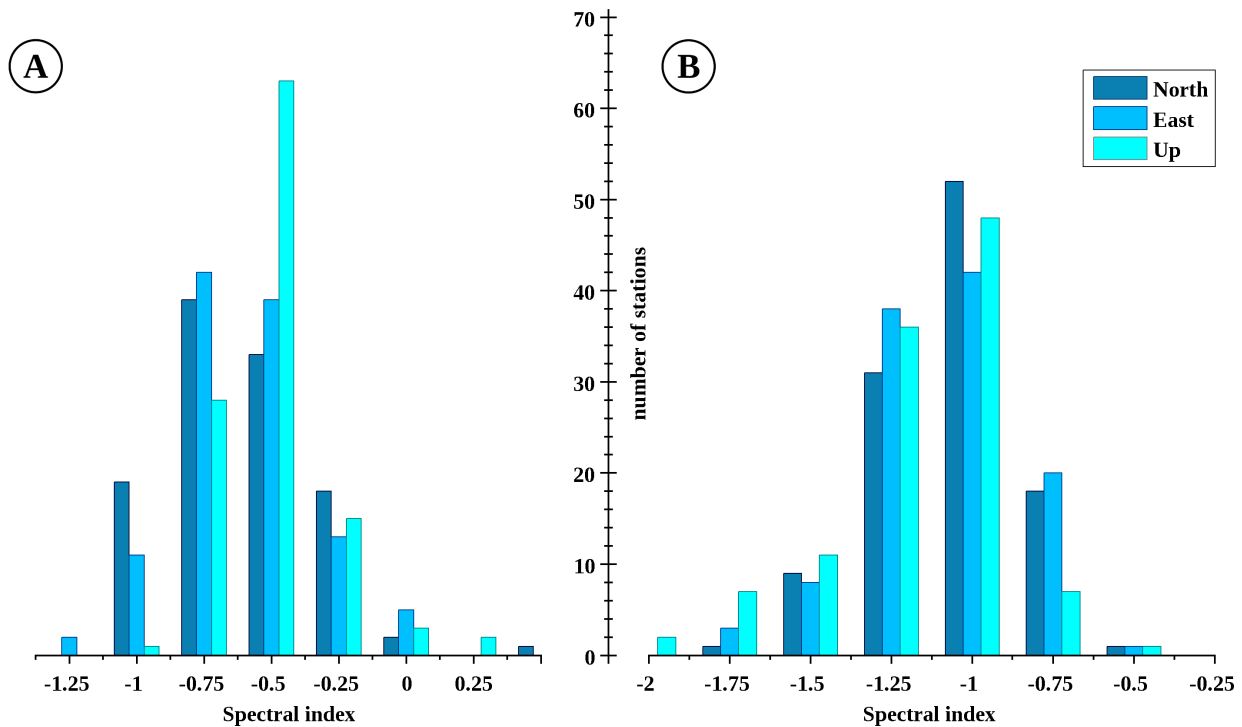
Figure 4: Histogram of the spectral indices estimated by (A) the spectral analysis, and (B) the Maximum Likelihood Estimation methods.

Although increasing the length of window makes the filtered spectrum smoother, surges of power at the above-mentioned specific periods become sharper. Spectral indices were estimated as −0.74, −0.72 and −0.61 for the north, east and up directions, respectively from the common power spectrum in the same way as for the individual spectra.

5.1.2 Maximum Likelihood Estimation

In order to consider a wider range of the power-law process, the spectral indices were estimated using the MLE method instead of constraining them to integers. We assumed the following power-law (PL) noise model:

$$\mathbf{C} = b_{PL\neq0}^2 \mathbf{J}_{PL} \tag{16}$$

and estimated spectral indices and noise amplitudes per station per direction for all stations using the CATS software Williams (2008). The reasons for choosing this model have been discussed in Williams et al. (2004).

Table 2 gives the numerical values of the estimated spectral indices, and Fig. 4B represents them in the form of a histogram. Spectral indices range from −1.70 to −0.53 for the north, from −1.81 to −0.54 for the east and from −1.96 to −0.54 for the up direction. The weighted averages

are −1.06 for the north, −1.10 for the east, and −1.18 for the up direction. Similar to the spectral analysis, the spectral characteristic of the noise is not significantly different among individual directions. The estimated ranges are between the fractional Gaussian and the fractional random-walk part of the noise spectrum (Fig. 1). Figure 4B shows that the estimated spectral indices for most of the stations are around −1 in all directions. This indicates prevalence of flicker noise model in the position time series. While results of both methods are in agreement, spectral indices obtained from the MLE are larger than those of the spectral analysis. This is primarily because in the PL noise model, spectral indices are left free to be estimated by maximizing the likelihood function that can bias the results to a value corresponding to the strongest noise model in the time series. Furthermore, spectral indices can be underestimated in the spectral analysis (a) for short time series Mao et al. (1999), and (b) as a result of decreasing relative power at lower frequencies due to removing trends, which have long periods (e.g., secular, annual and semi-annual trends) especially for shorter time series. In Table 2, stations with positive spectral indices estimated by spectral analysis (MEGR, GODR, GAS2, LONG, HDIL, and ACSO) have shortest lengths among all the position time series. Due to this fact, we do not calculate covariance matrices and consequently do not estimate velocities for this
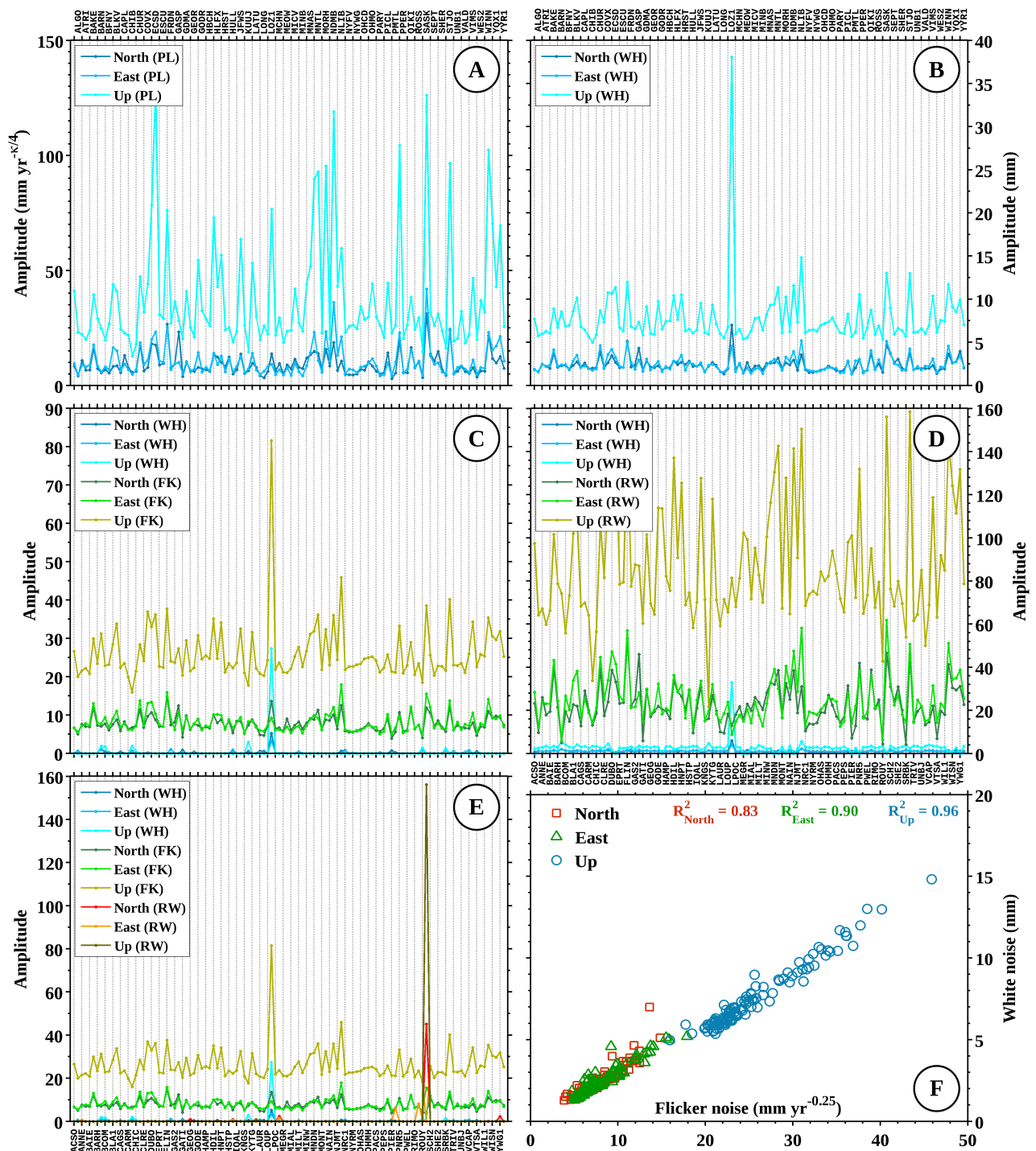
Figure 5: (A-E) Graphical representation of the estimated noise amplitudes in different models, (F) correlation of white noise versus flicker noise amplitudes for all stations except LOZ1.

noise model. Figure 5A represents the estimated noise amplitudes in this model. This figure shows that the noise amplitudes for the up direction are about 3–4 times (in average) larger than those of north and east directions indicating higher level of noise in the up direction. Amplitudes range between 3.0 and 31.2 mm $yr^{\kappa/4}$ (with the average of

9.3 mm $yr^{\kappa/4}$) for the north, 4.1 and 41.9 mm $yr^{\kappa/4}$ (with the average of 10.4 mm $yr^{\kappa/4}$) for the east, and 12.7 and 128.9 mm $yr^{\kappa/4}$ (with the average of 38.9 mm $yr^{\kappa/4}$) for the up direction.

We also fixed spectral indices to integer values in [−2, 0] and tested the following combination of noise models in

order to know what is the best describing noise model for the stochastic part of the position time series: white (WH), white plus flicker (WH+FL = WF), white plus random-walk (WH+RW = WR) and white plus flicker plus random-walk (WH+FK+RW = WFR). The advantages of assuming a specific type of noise model for all the time series have been discussed in Williams et al. (2004). Among them is the easier comparison of the noise characteristics of the time series when a parameter or noise model is held fixed. The best model in this concept is the one with maximum likelihood values. Following this assumption, we can expand the covariance matrix in Eq. (13) for the postulated models, respectively as:

$$\mathbf{C}_{WH} = a_{WH}^2 \mathbf{I} \tag{17}$$

$$\mathbf{C}_{WF} = a_W^2 \mathbf{I} + b_{FK}^2 \mathbf{J}_{FK} \tag{18}$$

$$\mathbf{C}_{WR} = a_W^2 \mathbf{I} + b_{RW}^2 \mathbf{J}_{RW} \tag{19}$$

$$\mathbf{C}_{WFR} = a_W^2 \mathbf{I} + b_{FK}^2 \mathbf{J}_{FK} + b_{RW}^2 \mathbf{J}_{RW} \tag{20}$$

with the same coefficients as in Eq. (13) where the subscripts denote the corresponding noise model.

The MLE values and the noise amplitudes were estimated from the postfit residuals using CATS software Williams (2008) per station per direction for all noise models. The MLE values were used to compare the models and choose the one that describes the best noise. Figure A.3 displays the result of comparison in terms of MLE differences, giving 6 comparisons. In other similar studies, all MLE values (in the case of few stations) or their summary (in the case of large number of stations, e.g., Williams et al. (2004)) are provided in a table format, but we preferred to present MLE differences graphically that makes it easier to compare different models especially when the number of CGPS stations is large. The figure shows WH and WF noise models have the minimum and the maximum MLE values, respectively, except in SASK where the WFR noise model is dominant. Therefore, WF is clearly the best noise model for describing the position time series. The WR noise model has the third rank among models. At stations where the difference between WH and WF, WR and WFR noise models is minimum (i.e., GODR, LONG, MEGR, MEOW, PIER, and SRBK), the length of time series is short.

The estimated noise amplitudes of the four models are represented in Fig. 5B–E. Overall, the noise amplitudes for the up direction are about 3–4 times (in average) larger than those of north and east directions indicating higher level of noise in the up direction. The nearly equal magnitude of north and east noise amplitudes is a good indi-

cator of essentially complete and successful phase ambiguity resolution Williams et al. (2004). The vertical direction of LOZ1 has the highest white and flicker noise amplitudes, which may be related to multipath and lack of direct sight to GPS satellites due to deep canopy shadow Sigrist et al. (1999). This station has been decommissioned since August 16, 2013 (Fig. A.1). However, due to having a good monument, its random-walk noise amplitude is low. The large random-walk noise amplitude of SASK in the up direction can be attributed to the monument instability of the station (Section 5.3). A meaningful correlation is observed between magnitudes of white and flicker noise amplitudes, shown in Fig. 5F. In this figure, R^2 is the coefficient of determination and shows how well the regression fits the data. The figure displays that not only there is a good correlation for individual directions, there is also a good overall correlation among all directions. The range of estimated noise amplitudes are summarized in Table 3.

We constructed the covariance matrices of the WF and the WFR noise models in Eq. (18) and Eq. (20) using the estimated noise amplitudes and approximated covariance matrices in Eq. (14) and Eq. (15), and calculated the uncertainties of the stations' velocities. The estimated uncertainties are shown in Table 2 in details and are summarized in Table 3. In the WH noise model, the information in the stochastic part of the position time series is discarded. Therefore, the estimated velocity uncertainties $\sigma_{\hat{a}}$ have smallest values among noise models due to the fact that they depend on the amplitude of the WH noise a_{WH}, number of epochs N and the length of time series T as Zhang et al. (1997):

$$\sigma_{\hat{a}(WH)}^2 \simeq \frac{12a^2}{\Delta T^2 \left(N^3 - N \right)} \tag{21}$$

for large N. The average of the WH noise amplitudes is at the level of ~2.5 mm for the horizontal and ~7.9 mm for the vertical directions, while the average of the estimated uncertainties is ~0.04 mm/yr for the horizontal and ~0.14 mm/yr for the vertical velocities. In the WF and WFR noise models, the flicker noise is stronger than other types of noise while the level of white noise is the same all over the study area.

The velocity uncertainty $\sigma_{\hat{a}}$ is estimated as Bos et al. (2008):

$$\sigma_{\hat{a}(FK)}^2 \simeq \frac{8 \, b_{-1}^2}{\pi \, \Delta T^{3/2} \left(N^2 - N \right)} \tag{22}$$

Table 2: Estimated spectral indices and velocity uncertainties.

No.	Station	Spectral indices						Velocity uncertainties (mm/yr) (WH/WF/WFR)		
		Spectral analysis			MLE			North	East	Up
		North	East	Up	North	East	Up			
1	ACSO	−0.02 ± 0.08	0.06 ± 0.08	−0.21 ± 0.08	−1.17	−1.25	−1.32	0.05/0.65/0.65	0.04/0.65/0.65	0.18/2.60/2.60
2	ALGO	−0.60 ± 0.04	−0.47 ± 0.04	−0.43 ± 0.04	−0.77	−0.79	−1.10	0.01/0.16/0.16	0.01/0.18/0.18	0.02/0.65/0.65
3	ANNE	−0.69 ± 0.06	−0.92 ± 0.06	−0.59 ± 0.05	−1.24	−1.15	−1.02	0.02/0.40/0.40	0.02/0.38/2.56	0.06/1.13/1.11
4	ATRI	−0.89 ± 0.05	−0.57 ± 0.04	−0.63 ± 0.04	−0.96	−1.03	−0.93	0.01/0.25/0.25	0.02/0.30/0.30	0.05/0.78/0.78
5	BAIE	−0.60 ± 0.05	−0.80 ± 0.05	−0.48 ± 0.05	−0.98	−1.13	−1.09	0.01/0.26/0.26	0.01/0.28/0.28	0.04/0.78/0.78
6	BAKE	−0.78 ± 0.05	−0.88 ± 0.05	−0.60 ± 0.05	−1.20	−1.21	−1.19	0.06/0.63/0.63	0.04/0.70/0.70	0.17/1.60/1.60
7	BARH	−0.59 ± 0.04	−0.49 ± 0.04	−0.52 ± 0.04	−1.00	−1.04	−1.15	0.02/0.26/0.26	0.02/0.28/0.28	0.07/0.84/0.84
8	BARN	−0.44 ± 0.05	−0.52 ± 0.05	−0.52 ± 0.04	−0.68	−0.70	−0.82	0.03/0.30/0.30	0.01/0.30/0.30	0.06/1.22/1.22
9	BCOM	−0.83 ± 0.08	−0.32 ± 0.08	−0.83 ± 0.08	−0.90	−0.90	−0.86	0.05/0.75/0.75	0.04/0.92/0.92	0.16/2.24/2.24
10	BFNY	−0.73 ± 0.05	−0.69 ± 0.05	−0.59 ± 0.05	−0.90	−1.02	−1.10	0.01/0.21/0.21	0.01/0.24/0.24	0.03/0.82/0.82
11	BLA1	−0.64 ± 0.06	−0.61 ± 0.06	−0.53 ± 0.05	−1.06	−1.43	−1.31	0.03/0.40/0.40	0.02/0.49/0.49	0.10/1.53/1.53
12	BLKV	−0.56 ± 0.04	−0.61 ± 0.04	−0.55 ± 0.04	−0.98	−1.22	−1.13	0.02/0.29/0.29	0.02/0.37/0.37	0.07/1.13/1.13
13	CAGS	−0.88 ± 0.04	−0.86 ± 0.04	−0.76 ± 0.04	−0.93	−0.95	−1.06	0.01/0.20/0.20	0.01/0.23/0.23	0.02/0.68/0.68
14	CAPL	−0.76 ± 0.05	−0.65 ± 0.05	−0.40 ± 0.04	−1.32	−1.12	−0.98	0.02/0.34/0.34	0.02/0.32/0.32	0.07/0.97/0.97
15	CARM	−0.57 ± 0.05	−0.73 ± 0.05	−0.40 ± 0.05	−1.13	−1.07	−1.06	0.03/0.31/0.31	0.02/0.33/0.33	0.09/0.99/0.99
16	CHIB	−0.61 ± 0.04	−0.48 ± 0.04	−0.73 ± 0.04	−0.83	−0.80	−0.75	0.01/0.23/0.23	0.01/0.21/0.21	0.03/0.55/0.55
17	CHIC	−0.59 ± 0.04	−0.42 ± 0.05	−0.65 ± 0.04	−0.89	−0.98	−0.87	0.02/0.28/0.28	0.01/0.26/0.26	0.05/0.89/0.89
18	CHUR	−1.06 ± 0.04	−0.98 ± 0.04	−0.50 ± 0.04	−1.30	−1.21	−1.36	0.01/0.33/0.33	0.01/0.39/0.39	0.04/0.81/0.81
19	CLRE	−0.70 ± 0.05	−0.65 ± 0.05	−0.58 ± 0.05	−0.96	−1.16	−1.19	0.02/0.27/0.27	0.01/0.29/0.29	0.04/0.90/0.90
20	COVX	−0.47 ± 0.05	−0.49 ± 0.05	−0.61 ± 0.05	−0.86	−0.88	−1.12	0.03/0.37/0.37	0.02/0.50/0.84	0.10/1.42/1.42
21	DUBO	−0.81 ± 0.04	−0.75 ± 0.04	−0.70 ± 0.04	−1.37	−1.28	−1.62	0.01/0.31/0.31	0.01/0.38/0.38	0.04/0.95/0.95
22	ECSD	−0.23 ± 0.07	−0.29 ± 0.08	−0.48 ± 0.08	−1.51	−1.60	−1.96	0.08/0.86/0.86	0.07/1.01/1.01	0.26/3.57/3.57
23	EPRT	−0.67 ± 0.05	−0.67 ± 0.05	−0.64 ± 0.05	−1.17	−1.24	−1.21	0.04/0.37/0.37	0.02/0.34/0.34	0.13/1.21/1.21
24	ESCU	−0.63 ± 0.05	−0.67 ± 0.05	−0.41 ± 0.05	−1.22	−1.26	−1.18	0.02/0.32/0.32	0.01/0.32/0.32	0.05/1.02/1.02
25	FLIN	−1.01 ± 0.04	−0.71 ± 0.04	−0.65 ± 0.04	−1.41	−1.32	−1.50	0.02/0.46/0.46	0.02/0.49/0.49	0.07/1.17/1.17
26	FRDN	−0.66 ± 0.05	−0.68 ± 0.05	−0.52 ± 0.05	−1.03	−0.75	−1.08	0.04/0.35/0.35	0.03/0.43/0.43	0.12/1.15/1.15
27	GAS2	−0.39 ± 0.10	0.11 ± 0.10	0.07 ± 0.10	−1.10	−1.30	−1.30	0.09/1.28/1.28	0.13/1.13/1.13	0.55/4.32/4.32
28	GASP	−0.55 ± 0.11	−0.44 ± 0.10	−0.22 ± 0.10	−1.45	−0.95	−1.02	0.09/1.78/1.78	0.07/1.53/1.53	0.30/3.91/3.91
29	GATI	−0.92 ± 0.07	−0.72 ± 0.07	−0.79 ± 0.07	−0.74	−0.87	−1.00	0.04/0.39/0.39	0.03/0.54/0.54	0.09/1.75/1.75
30	GDMA	−0.73 ± 0.05	−0.66 ± 0.05	−0.64 ± 0.05	−1.02	−1.07	−1.23	0.01/0.34/0.34	0.01/0.33/0.33	0.05/1.02/1.02
31	GEOG	−1.03 ± 0.06	−0.80 ± 0.06	−0.58 ± 0.06	−1.03	−0.95	−1.11	0.02/0.40/3.70	0.02/0.42/0.41	0.08/1.39/1.36

Continued on next page

Table 2: ...continued

| No. | Station | Spectral indices | | | | | | Velocity uncertainties (mm/yr) | | |
| | | Spectral analysis | | | MLE | | | (WH/WF/WFR) | | |
		North	East	Up	North	East	Up	North	East	Up
32	GEOR	−0.46 ± 0.08	−0.66 ± 0.08	−0.20 ± 0.08	−0.83	−0.95	−0.96	0.12/1.00/1.00	0.09/1.01/1.01	0.41/2.90/2.90
33	GODE	−0.65 ± 0.04	−0.81 ± 0.04	−0.75 ± 0.04	−1.05	−1.33	−1.40	0.01/0.21/0.21	0.01/0.26/0.26	0.03/0.89/0.89
34	GODR	−0.25 ± 0.15	0.03 ± 0.14	0.36 ± 0.12	−1.07	−0.96	−1.19	0.15/1.63/1.63	0.12/1.54/1.54	0.51/6.16/6.16
35	HAMP	−0.68 ± 0.05	−0.95 ± 0.05	−0.58 ± 0.05	−1.00	−1.06	−1.09	0.01/0.25/0.25	0.01/0.26/0.26	0.04/0.92/0.92
36	HBCH	−0.73 ± 0.05	−0.55 ± 0.05	−0.64 ± 0.05	−0.95	−0.96	−1.03	0.01/0.24/0.24	0.01/0.25/0.25	0.04/0.92/0.92
37	HDIL	−0.27 ± 0.07	0.11 ± 0.08	−0.58 ± 0.08	−1.20	−1.23	−1.52	0.14/1.29/1.29	0.11/1.29/1.29	0.31/3.88/3.88
38	HLFX	−0.73 ± 0.05	−0.55 ± 0.05	−0.77 ± 0.05	−1.31	−0.92	−1.39	0.01/0.30/0.30	0.01/0.39/0.38	0.05/0.93/2.00
39	HNPT	−0.77 ± 0.04	−0.93 ± 0.04	−0.57 ± 0.04	−1.08	−1.18	−1.36	0.02/0.31/0.31	0.02/0.36/0.36	0.09/1.24/1.24
40	HRST	−1.02 ± 0.05	−0.49 ± 0.05	−0.58 ± 0.05	−1.14	−0.96	−1.09	0.03/0.35/0.35	0.02/0.33/0.33	0.10/1.11/1.11
41	HSTP	−0.97 ± 0.05	−0.78 ± 0.05	−0.65 ± 0.05	−1.26	−1.20	−1.05	0.02/0.32/0.32	0.02/0.33/0.33	0.07/0.89/0.89
42	HULL	−1.02 ± 0.06	−0.84 ± 0.06	−0.63 ± 0.06	−0.83	−0.82	−0.89	0.02/0.34/3.45	0.02/0.41/2.79	0.08/1.41/1.37
43	IQAL	−0.25 ± 0.07	−0.49 ± 0.07	−0.37 ± 0.07	−0.86	−1.03	−1.00	0.09/0.87/0.87	0.06/0.84/0.84	0.14/2.19/2.19
44	JFWS	−0.10 ± 0.08	−0.19 ± 0.08	−0.11 ± 0.07	−1.36	−1.21	−1.49	0.07/0.89/0.89	0.06/1.01/1.01	0.27/3.49/3.49
45	KNGS	−0.65 ± 0.06	−0.80 ± 0.05	−0.56 ± 0.05	−0.98	−1.03	−1.15	0.01/0.25/0.25	0.01/0.24/0.24	0.04/0.98/0.98
46	KUUJ	−0.72 ± 0.05	−0.71 ± 0.05	−0.77 ± 0.05	−0.88	−0.91	−0.71	0.03/0.36/0.36	0.02/0.40/0.40	0.10/0.87/0.87
47	KYTG	−0.81 ± 0.06	−0.50 ± 0.07	−0.45 ± 0.07	−1.07	−1.36	−1.37	0.03/0.57/0.57	0.03/0.55/0.55	0.11/2.04/2.04
48	LATU	−0.82 ± 0.06	−1.14 ± 0.06	−0.59 ± 0.06	−1.07	−0.99	−1.21	0.02/0.42/0.42	0.02/0.40/0.40	0.08/1.30/3.80
49	LAUR	−0.74 ± 0.06	−0.71 ± 0.05	−0.72 ± 0.05	−0.82	−0.85	−0.97	0.01/0.23/0.23	0.01/0.28/0.28	0.04/0.95/0.95
50	LONG	−0.15 ± 0.09	−0.27 ± 0.09	0.12 ± 0.08	−0.68	−1.05	−1.17	0.12/0.91/0.91	0.09/1.12/1.12	0.41/3.94/3.94
51	LOUP	−0.63 ± 0.06	−0.49 ± 0.05	−0.60 ± 0.05	−0.90	−1.09	−0.94	0.02/0.35/0.35	0.02/0.37/0.37	0.09/1.23/1.23
52	LOZ1	−0.70 ± 0.06	−0.70 ± 0.06	−0.62 ± 0.06	−0.53	−0.54	−0.54	0.08/1.25/1.25	0.06/0.84/0.84	0.67/8.58/8.58
53	LPOC	−0.73 ± 0.06	−0.25 ± 0.05	−0.42 ± 0.05	−0.98	−0.82	−1.00	0.02/0.34/0.34	0.02/0.32/0.32	0.07/1.14/1.14
54	MCHN	−1.06 ± 0.08	−1.25 ± 0.08	−0.36 ± 0.08	−1.25	−1.07	−1.15	0.05/0.62/10.68	0.04/0.57/6.53	0.17/2.19/1.92
55	MEGR	0.58 ± 0.13	−0.14 ± 0.14	0.15 ± 0.15	−0.90	−0.85	−0.92	0.21/1.88/1.88	0.16/1.88/1.88	0.67/7.09/7.09
56	MEOW	−0.59 ± 0.13	−0.52 ± 0.12	−0.28 ± 0.12	−1.00	−1.06	−1.08	0.18/2.16/2.16	0.14/1.67/1.67	0.61/5.05/5.05
57	MIAL	−0.50 ± 0.05	−0.23 ± 0.05	−0.64 ± 0.05	−1.12	−0.86	−1.06	0.05/0.45/0.45	0.04/0.50/0.50	0.17/1.72/1.72
58	MICV	−0.62 ± 0.05	−0.41 ± 0.06	−0.71 ± 0.06	−1.31	−1.27	−1.36	0.02/0.38/0.38	0.02/0.34/0.34	0.07/1.31/1.31
59	MILT	−0.53 ± 0.05	−0.66 ± 0.05	−0.51 ± 0.05	−0.97	−0.84	−0.99	0.03/0.38/0.38	0.02/0.33/0.33	0.24/2.13/2.13
60	MINB	−0.37 ± 0.06	−0.27 ± 0.06	−0.32 ± 0.06	−1.09	−0.83	−1.03	0.07/0.67/0.67	0.05/0.45/0.45	0.19/2.08/2.08
61	MINW	−0.91 ± 0.05	−0.77 ± 0.05	−0.46 ± 0.05	−1.30	−1.12	−1.36	0.04/0.42/0.42	0.02/0.35/0.35	0.07/1.28/1.28
62	MNAS	−0.24 ± 0.09	−0.41 ± 0.09	−0.34 ± 0.08	−1.28	−1.34	−1.37	0.09/1.04/1.04	0.07/1.02/1.02	0.28/3.58/3.58
63	MNDN	−0.57 ± 0.08	−0.25 ± 0.09	−0.38 ± 0.08	−1.36	−1.61	−1.75	0.22/1.15/1.15	0.18/1.28/1.28	0.36/3.76/3.76

Continued on next page

Table 2: ...continued

| No. | Station | Spectral indices | | | | | | Velocity uncertainties (mm/yr) (WH/WF/WFR) | | |
| | | Spectral analysis | | | MLE | | | | | |
		North	East	Up	North	East	Up	North	East	Up
64	MNTL	−0.36 ± 0.07	−0.34 ± 0.07	−0.42 ± 0.07	−1.15	−1.11	−1.70	0.07/0.86/0.86	0.08/0.75/0.75	0.44/3.10/3.10
65	MONT	−0.92 ± 0.04	−0.78 ± 0.04	−0.50 ± 0.04	−1.06	−0.94	−1.03	0.02/0.26/0.26	0.02/0.26/0.26	0.07/0.91/0.91
66	MORH	−0.42 ± 0.07	−0.76 ± 0.07	−0.53 ± 0.07	−1.42	−1.61	−1.80	0.09/0.79/0.79	0.08/0.90/0.90	0.28/2.92/2.92
67	NAIN	−0.65 ± 0.05	−0.77 ± 0.05	−0.55 ± 0.05	−0.99	−1.06	−0.92	0.02/0.34/0.34	0.01/0.39/0.39	0.04/0.85/0.85
68	NDMB	−0.39 ± 0.06	−0.70 ± 0.06	−0.32 ± 0.05	−1.44	−1.81	−1.88	0.03/0.53/0.53	0.06/0.72/0.72	0.10/1.87/1.87
69	NJMT	−0.36 ± 0.05	−0.46 ± 0.05	−0.57 ± 0.05	−1.01	−1.37	−1.40	0.07/0.42/0.42	0.06/0.51/0.51	0.16/1.45/1.45
70	NLIB	−0.70 ± 0.05	−0.92 ± 0.05	−0.83 ± 0.05	−0.87	−1.11	−1.18	0.05/0.62/0.62	0.04/0.88/0.88	0.19/2.26/2.26
71	NRC1	−0.59 ± 0.04	−0.66 ± 0.04	−0.53 ± 0.04	−0.75	−0.79	−1.04	0.03/0.25/0.25	0.03/0.28/0.28	0.10/0.89/0.89
72	NYFV	−0.35 ± 0.05	−0.71 ± 0.06	−0.60 ± 0.06	−0.88	−1.14	−1.09	0.04/0.33/0.33	0.03/0.37/0.37	0.05/1.16/1.16
73	NYRM	−0.50 ± 0.06	−0.66 ± 0.06	−0.40 ± 0.06	−0.88	−1.13	−1.11	0.01/0.28/0.28	0.01/0.29/0.29	0.05/1.16/1.16
74	NYWG	−0.15 ± 0.07	−0.20 ± 0.07	−0.25 ± 0.07	−0.90	−0.95	−1.04	0.03/0.44/0.44	0.02/0.46/0.46	0.09/1.77/1.77
75	OHAS	−0.34 ± 0.06	−0.61 ± 0.06	−0.43 ± 0.06	−1.08	−1.20	−1.27	0.04/0.37/0.37	0.03/0.35/0.35	0.12/1.39/1.39
76	OHCD	−0.33 ± 0.06	−0.58 ± 0.06	−0.53 ± 0.06	−0.99	−1.16	−1.10	0.04/0.39/0.39	0.03/0.37/0.37	0.17/1.67/1.67
77	OHMH	−0.51 ± 0.05	−0.59 ± 0.05	−0.46 ± 0.05	−1.19	−1.19	−1.12	0.04/0.53/0.53	0.02/0.28/0.28	0.10/0.99/0.99
78	OHMO	−0.50 ± 0.05	−0.69 ± 0.06	−0.58 ± 0.05	−1.16	−1.38	−1.40	0.04/0.41/0.41	0.03/0.42/0.42	0.14/1.54/1.54
79	PACS	−0.54 ± 0.07	−0.54 ± 0.07	−0.47 ± 0.07	−1.03	−1.15	−1.15	0.04/0.48/0.48	0.03/0.56/0.56	0.12/1.97/1.97
80	PARY	−0.42 ± 0.05	−0.78 ± 0.05	−0.58 ± 0.05	−0.91	−0.87	−1.14	0.02/0.29/0.29	0.02/0.26/0.26	0.06/1.09/1.09
81	PEPS	−0.48 ± 0.06	−0.30 ± 0.06	−0.60 ± 0.06	−0.90	−0.87	−0.95	0.02/0.42/0.42	0.01/0.36/0.36	0.06/1.43/1.43
82	PICL	−0.67 ± 0.05	−0.61 ± 0.05	−0.79 ± 0.05	−1.32	−0.98	−1.39	0.03/0.40/0.40	0.02/0.47/0.47	0.08/1.14/1.14
83	PIER	−0.20 ± 0.09	−0.49 ± 0.09	−0.20 ± 0.09	−0.63	−0.87	−1.04	0.05/0.54/0.54	0.04/0.70/0.70	0.17/2.96/2.96
84	PMTL	−0.85 ± 0.06	−0.87 ± 0.07	−0.49 ± 0.07	−0.97	−1.30	−1.15	0.03/0.38/0.32	0.05/0.52/23.33	0.21/1.59/1.36
85	PNR5	−0.37 ± 0.07	−0.52 ± 0.07	−0.59 ± 0.06	−1.43	−1.63	−1.84	0.05/0.76/0.76	0.04/0.69/0.69	0.16/2.37/2.37
86	PPER	−0.46 ± 0.06	−0.38 ± 0.06	−0.21 ± 0.06	−0.98	−1.01	−0.99	0.04/0.46/0.46	0.03/0.40/0.40	0.13/1.66/1.66
87	PWEL	−0.73 ± 0.06	−0.98 ± 0.06	−0.80 ± 0.05	−0.93	−1.13	−1.09	0.03/0.32/0.32	0.02/0.30/0.30	0.08/1.19/1.19
88	QIKI	−0.78 ± 0.05	−0.82 ± 0.05	−0.65 ± 0.05	−1.24	−1.17	−1.19	0.03/0.50/0.50	0.02/0.52/0.52	0.08/1.24/1.24
89	RIMO	−0.40 ± 0.05	−0.66 ± 0.05	−0.61 ± 0.05	−1.13	−1.17	−1.12	0.01/0.29/0.29	0.01/0.28/0.28	0.04/0.93/0.93
90	ROSS	−1.12 ± 0.06	−1.03 ± 0.06	−0.67 ± 0.05	−1.24	−1.25	−1.16	0.05/0.41/0.34	0.04/0.41/24.73	0.17/1.30/1.10
91	ROUY	−0.53 ± 0.04	−0.96 ± 0.05	−0.68 ± 0.04	−0.65	−0.78	−0.80	0.01/0.17/0.16	0.01/0.20/2.12	0.05/0.76/0.75
92	SASK	−1.06 ± 0.05	−0.53 ± 0.05	−0.58 ± 0.05	−1.70	−1.71	−1.83	0.02/0.45/83.32	0.02/0.59/0.34	0.08/1.45/288.49
93	SCH2	−0.91 ± 0.04	−0.98 ± 0.04	−0.98 ± 0.04	−1.18	−1.04	−1.15	0.05/0.42/0.42	0.04/0.51/0.51	0.15/1.02/1.02
94	SEPT	−1.09 ± 0.06	−0.85 ± 0.06	−0.49 ± 0.05	−1.27	−1.22	−1.17	0.02/0.36/0.36	0.02/0.33/0.33	0.07/1.02/1.02
95	SHE2	−0.98 ± 0.06	−0.76 ± 0.06	−0.45 ± 0.06	−1.39	−1.15	−1.21	0.07/0.58/0.58	0.05/0.54/0.54	0.15/1.44/1.44

Table 2: ...continued

No.	Station	Spectral indices						Velocity uncertainties (mm/yr) (WH/WF/WFR)		
		Spectral analysis			MLE					
		North	East	Up	North	East	Up	North	East	Up
96	SHER	-0.72 ± 0.06	-0.56 ± 0.05	-0.58 ± 0.05	-1.00	-0.92	-1.03	0.02/0.35/0.35	0.01/0.34/0.34	0.06/1.18/1.18
97	SRBK	-0.79 ± 0.09	-0.02 ± 0.08	-0.41 ± 0.08	-0.69	-0.71	-0.78	0.06/0.77/0.77	0.04/0.88/0.88	0.17/2.92/2.92
98	STJO	-0.73 ± 0.05	-0.47 ± 0.04	-0.49 ± 0.04	-1.49	-1.41	-1.63	0.04/0.46/0.46	0.03/0.48/0.48	0.14/1.46/1.46
99	TRIV	-0.70 ± 0.05	-0.80 ± 0.04	-0.69 ± 0.04	-0.83	-0.81	-0.88	0.02/0.24/0.24	0.01/0.24/0.24	0.05/0.91/0.91
100	UNB1	-0.71 ± 0.07	-0.47 ± 0.07	-0.51 ± 0.06	-0.89	-0.98	-0.93	0.04/0.62/0.62	0.03/0.69/0.69	0.12/1.94/1.94
101	UNBJ	-0.69 ± 0.06	-0.61 ± 0.05	-0.40 ± 0.06	-1.14	-1.22	-1.22	0.03/0.39/0.39	0.04/0.40/0.40	0.15/1.50/1.50
102	VALD	-0.55 ± 0.05	-0.68 ± 0.05	-0.79 ± 0.05	-0.91	-0.93	-0.91	0.05/0.35/0.35	0.03/0.40/0.40	0.11/0.99/0.99
103	VCAP	-0.68 ± 0.04	-0.63 ± 0.04	-0.39 ± 0.04	-0.78	-0.78	-0.89	0.02/0.24/0.24	0.01/0.24/0.24	0.07/1.08/1.08
104	VIMS	-0.56 ± 0.05	-0.54 ± 0.05	-0.45 ± 0.05	-0.98	-1.04	-1.22	0.04/0.39/0.39	0.02/0.42/0.42	0.09/1.38/1.38
105	VTSA	-0.33 ± 0.06	-0.34 ± 0.06	-0.17 ± 0.06	-0.77	-0.92	-0.92	0.02/0.31/0.31	0.02/0.36/0.36	0.07/1.49/1.49
106	WES2	-0.39 ± 0.04	-0.40 ± 0.04	-0.40 ± 0.04	-0.93	-1.00	-1.25	0.02/0.27/0.27	0.02/0.31/0.31	0.11/1.05/1.05
107	WIL1	-0.66 ± 0.04	-0.62 ± 0.04	-0.40 ± 0.04	-0.93	-1.02	-1.16	0.02/0.25/0.25	0.02/0.26/0.26	0.07/0.88/0.88
108	WINN	-0.98 ± 0.04	-0.80 ± 0.04	-0.65 ± 0.04	-1.48	-1.35	-1.76	0.03/0.37/0.37	0.04/0.52/0.52	0.09/1.19/1.19
109	WISN	-0.23 ± 0.07	-0.48 ± 0.08	-0.33 ± 0.07	-1.17	-1.37	-1.60	0.08/0.94/0.94	0.06/0.93/0.93	0.26/3.10/3.10
110	YQX1	-0.36 ± 0.07	-0.43 ± 0.06	-0.47 ± 0.07	-1.00	-1.46	-1.26	0.04/0.65/0.65	0.03/0.61/0.61	0.12/1.99/1.99
111	YWG1	-1.02 ± 0.06	-1.04 ± 0.07	-0.44 ± 0.06	-1.21	-1.57	-1.57	0.09/0.74/9.73	0.07/0.77/0.73	0.28/2.52/2.38
112	YYR1	-0.49 ± 0.07	-0.61 ± 0.07	-0.33 ± 0.07	-1.01	-1.31	-1.01	0.03/0.51/0.51	0.03/0.48/0.48	0.10/1.77/1.77

Concluded

Table 3: Summary of the estimated amplitudes for the different noise models and their velocity uncertainties.

Noise model		WH (mm)			FK (mm yr$^{-0.25}$)			RW (mm yr$^{-0.5}$)			Velocity uncertainties (mm/yr)		
		North	East	Up	North	East	Up	North	East	Up	North	East	Up
WH	Min.	1.28	1.30	4.97							0.01	0.01	0.02
	Max.	6.99	5.20	38.06							0.22	0.18	0.67
	Mean	2.38	2.45	7.86							0.04	0.03	0.14
WR	Min.	0.53	0.00	0.00				4.15	5.79	21.71			
	Max.	6.00	3.87	32.90				53.34	61.80	158.49			
	Mean	1.08	1.02	2.89				22.61	25.19	87.46			
WF	Min.	0.00	0.00	0.00	3.86	4.75	15.93				0.16	0.18	0.55
	Max.	5.17	3.28	27.32	14.84	17.89	81.57				2.16	1.88	8.58
	Mean	0.16	0.11	0.35	7.65	8.06	26.19				0.51	0.53	1.77
WFR	Min.	0.00	0.00	0.00	3.86	4.71	0.00	0.00	0.00	0.00	0.16	0.18	4.35
	Max.	5.17	3.28	27.32	14.84	17.89	81.57	45.10	8.14	156.15	83.32	24.73	288.49
	Mean	0.16	0.11	0.35	7.58	8.06	25.84	0.46	0.16	1.41	1.48	1.06	4.35

for the flicker noise, and as Williams (2003); Zhang et al. (1997):

$$\sigma_{\hat{a}_{(RW)}}^2 \simeq \frac{b_{-2}^2}{\Delta T (N-1)} = \frac{b_{-2}^2}{T} \tag{23}$$

for the random-walk noise, when $N \geq 2$. In both models, the average of the flicker noise amplitude is at the level of ~8 mm yr$^{-0.25}$ for the horizontal and ~26 mm yr$^{-0.25}$ for the vertical directions. This is while the average of the estimated uncertainties in the WF noise model is at the level of ~0.5 mm/yr for the horizontal and ~1.8 mm/yr for the vertical velocities. In the WFR noise model, the average of the random-walk noise amplitude is at the level of ~0.5 mm yr$^{-0.5}$ for the horizontal and ~1.4 mm yr$^{-0.5}$ for the vertical directions, while the average of the estimated uncertainties in the WFR noise model is at the level of ~1.5 mm/yr for the horizontal and ~4.4 mm/yr for the vertical velocities. Velocity uncertainties obtained from the WF noise model have increased by a factor of 5 for MNDN and 38 for DUBO stations, compared with those obtained from the WH noise model. For most of the stations, velocity uncertainties in the east direction increased more compared with the other directions for the same station.

5.2 Spatial correlation of estimated amplitudes

We analyzed spatial distribution of flicker noise amplitudes across our CGPS network. The network extends 31°N in latitude (36°N–67°N) and 54°W in longitude (52°W–106°W). Stations are neither evenly distributed in latitude nor longitude, however, most of the stations are located in the SLRV area (Fig. 2) between 40°N–50°N and 65° W–85°W.

Figure 6 represents flicker noise amplitudes for the north, east and up directions as a function of stations' latitude and longitude. The relationship is approximated by a best fitting quadratic trend obtained from the weighted least-squares method for each graph. The figure shows that the level of noise in the vertical direction is 2 to 5 times larger than those in horizontal directions. Furthermore, it shows that estimated amplitudes are spatially correlated in both latitude and longitude directions, despite the relatively low values of R^2 and small numbers of CGPS stations at higher latitudes. The noise behavior in the latitude direction is, however, slightly different with the longitude direction. While in the former direction, the noise amplitude is larger in higher latitudes and decreases in lower latitudes for horizontal directions, it is minimum at mid-latitudes and maximum at lower and higher latitudes for the latter direction. In the longitude direction, the noise

amplitude is minimum for all components over the area where CGPS stations are aggregated. The coefficient of determination is 3–4 times larger in this direction for all components.

The fact that the noise amplitude is latitude dependent in global solutions was already shown in the literature. Mao et al. (1999) found significantly higher levels of white noise in the vertical direction of the tropical stations. Williams et al. (2004) showed that both white and flicker noise components have latitude dependency in their amplitudes and are maximum at the equator, however, the flicker noise is not as convincingly as the white noise. The latitude dependency was also observed by Williams and Willis (2006) in the weekly station coordinate time series of DORIS observations, which is best described by a combination of variable white noise plus flicker noise. In this case, while the variable white noise shows dependency on station latitude and the number of satellites used in the solution, the flicker noise amplitude does not show dependency on latitude. The regional correlations are attributed to mismodeling due to tropospheric water vapor Dixon and Kornreich Wolf (1990), the first-order ionospheric phase advance and group delay Montillet et al. (2013) and the near polar satellites' orbit in the case of the DORIS time series Williams and Willis (2006).

The difference between our regional scale results and global scale solutions is related to the GPS data processing method. As stated earlier, even if not completely understood, the noise in the CGPS time series is normally attributed to imperfections of the models used in the data processing. In the differential processing methods, many known or unknown errors are completely eliminated (e.g., satellites clock error) or greatly reduced (e.g., ionospheric and tropospheric errors), especially for not far away stations Xu (2007, p. 108). Therefore, the noise is significantly reduced over the central part of the network due to many short baselines that are formed in the double-difference data processing method. However, other sources of error such as known random atmospheric effects could dominate the error budget due to longer interstation spacing in regional GPS networks Williams et al. (2004).

5.3 Stability of monuments

One of the objectives behind this study, as stated in Section 1, is to evaluate the stability of different types of monuments of the CGPS network. Although we are generally interested to know the velocity of the earth's crust units, what is actually measured is the displacement of a monument on or just below the earth's surface. The monument
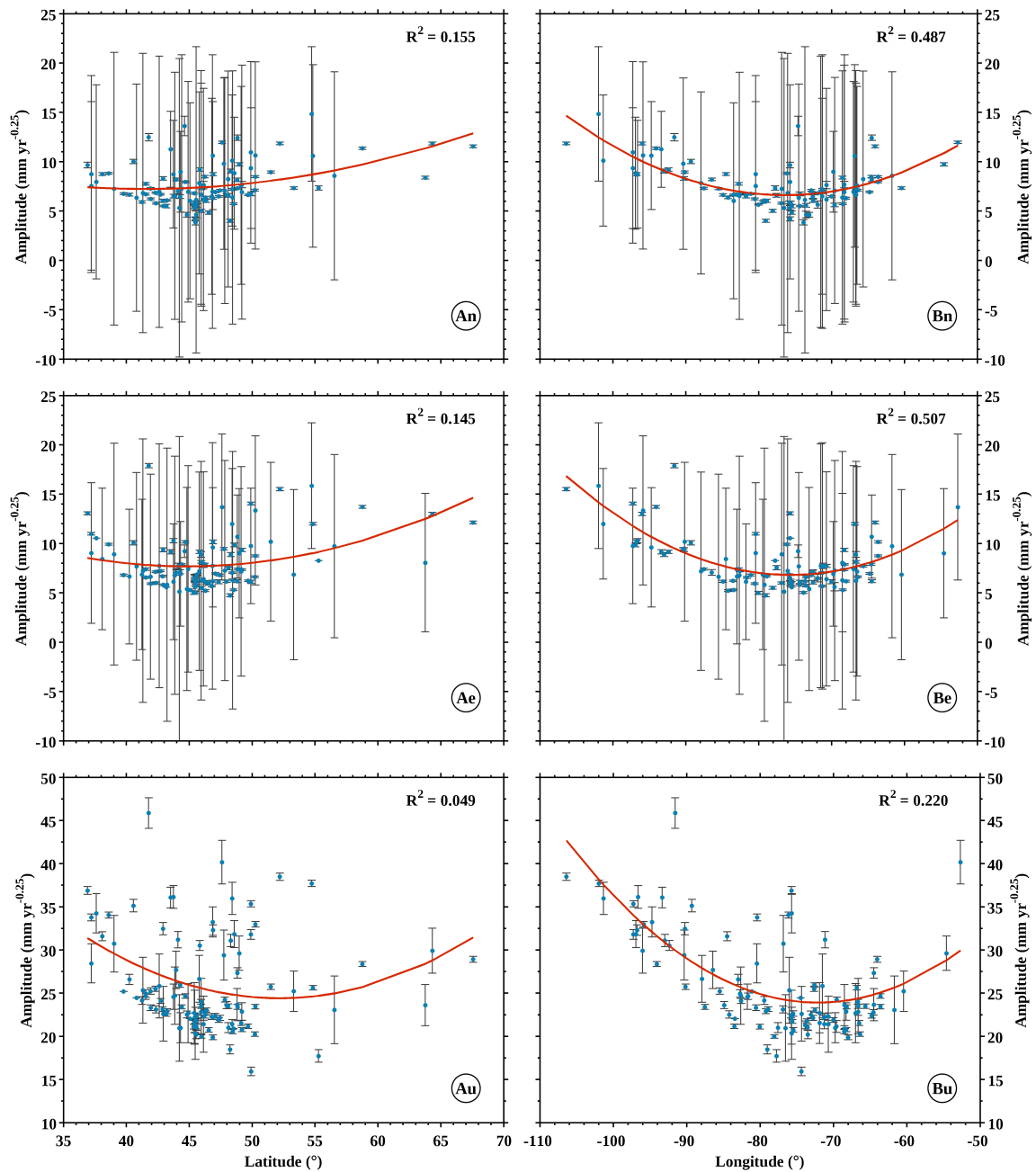
Figure 6: Flicker noise amplitudes as a function of (A) station latitude, and (B) station longitude for the north (n), east (e) and up (u) directions as well as their one-sigma uncertainties and the quadratic trend in the least-squares sense.

noise resulted from nontectonic movement of the monument has been identified as an important source of noise in many geodetic data sets Johnson and Agnew (1995); Langbein et al. (1995), and has been proven to be a random-walk process Langbein and Johnson (1997). Therefore, we applied the WFR noise model to estimate the amplitude of the random-walk noise. While it is zero for most of them, few millimeters of random-walk amplitude is observed for some stations as presented in Table 4 that is attributed

to the physical instability in the monuments of CGPS stations. The evidence for this is discussed in Beavan (2005). Figure 7 shows the spatial distribution of the stations with non-zero random-walk amplitude. The high values of the random-walk amplitude in station SASK for north and up directions are noticeable in Table 4.

The amplitude of random-walk noise is zero for other stations not listed in Table 4. However, this does not imply the lack of random-walk noise in these stations due

Table 4: Random-walk noise amplitude and minimum length of time series necessary to detect the corresponding noise amplitude.

| No.	Station	RW (mm yr$^{-0.5}$)			Len. (yr)	Estimated len. (yr)		
		North	East	Up		North	East	Up
1	ANNE*	0.00	0.66	0.00	8.73	-	9.2	-
2	COVX*	0.00	0.20	0.00	12.42	-	100.0	-
3	GEOG	0.88	0.00	0.00	6.79	5.2	-	-
4	HLFX*	0.00	0.00	0.53	11.53	-	14.2	-
5	HULL*	0.79	0.63	0.00	7.32	6.4	10.1	-
6	LATU	0.00	0.00	0.86	7.49	-	-	5.4
7	MCHN	2.35	1.43	0.00	4.49	0.7	2.0	-
8	PMTL	0.00	6.17	0.00	6.2	-	0.1	-
9	ROSS	0.00	8.14	0.00	8.99	-	0.1	-
10	ROUY*	0.00	0.62	0.00	13.48		10.4	-
11	SASK	45.10	0.00	156.15	11.15	~0	-	~0
12	YWG1	2.23	0.00	0.00	6.18	0.8	-	-
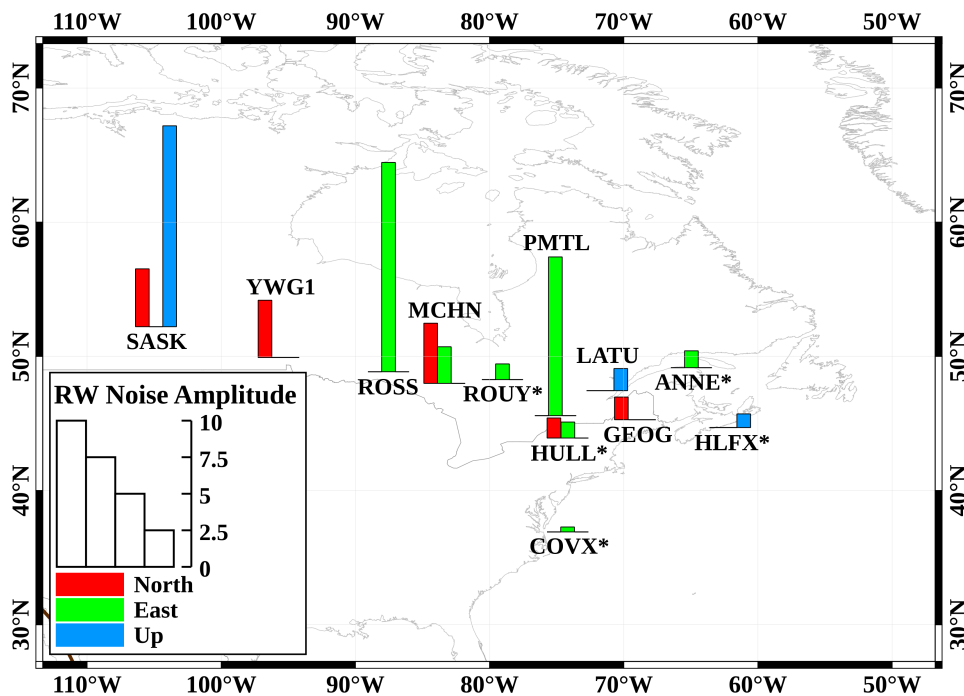
Figure 7: Spatial distribution of the stations with non-zero random-walk amplitude. The scale for SASK is 1/20.

to the fact that, in general, the amplitude of the random-walk noise in the geodetic quality monuments is less than 0.5 mm yr$^{-0.5}$ King and Williams (2009) and can be underestimated (a) when it has considerably lower magnitude compared with flicker or white noises Klos et al. (2014), or (b) when the length of time series is short. This problem in the MLE has been reported by Zhang et al. (1997). Dmitrieva and Segall (2015) discuss that the MLE fails to detect random-walk noise if its magnitude (e.g., 0.38 mm yr$^{-0.5}$) is significantly lower than flicker noise

(e.g., 2 mm yr$^{-0.25}$). They developed a network noise estimator to detect the colored noise properties of CGPS position time series in regions of low deformation rates in which all stations are processed simultaneously by a Kalman filter and using the MLE to solve for the best fitting variance parameters in the noise model. This fact is, however, contrary in the literature. Langbein and Johnson (1997) has evaluated accuracy of the MLE using two synthetic time series containing the white noise of 1 mm and the random-walk noise of 0.5, 1.5 and 4.0 mm yr$^{-0.5}$.

Their results show accurate measure of both noise components and uncertainties by the MLE. Williams et al. (2004) have tested the MLE on synthetic time series with different lengths. They conclude that the accuracy of the estimated spectral indices depends on the ratio of the colored noise and the white noise amplitudes, the length of time series, and a trade-off between the trend due to tectonic motion and the trend due to the noise in the time series.

Williams et al. (2004) state that to detect a random-walk noise in a monument with an amplitude of about 0.4 mm $yr^{-0.5}$, the position time series would have to be 30 years long. This is equivalent to detecting a typical displacement of 2 mm, reliably. In this way, we calculated the minimum length of time series for stations in Table 4 that is necessary for detecting the corresponding random-walk noise. Stations with an asterisk have shorter time series than the calculated length. Therefore, the detected random-walk noise is not reliable enough to rule out these stations.

6 Conclusion

We analyzed the noise behavior of 112 CGPS stations in eastern North America using the spectral analysis and the MLE methods. Both methods showed prevalence of the white plus flicker noise in the position time series. The noise amplitude is highest in the up and lowest in the north direction for all tested models. Velocity uncertainties were estimated for WH, WF and WFR noise models using the MLE method. They are smaller or underestimated in the WH noise model due to the fact that the time-dependent characteristics of the position time series are neglected. Velocity uncertainties in the WF and WFR noise models are the same for most of the stations, but they are all increased by a factor of 5–38 compared to the WH noise model. The largest uncertainties are obtained from the WFR noise model. We found 7 stations with few millimeters of random-walk amplitude attributed to the physical instability in their monuments. Undetectable random-walk noise at the other stations does not necessarily indicate a perfect stability, but longer time series are required to accurately assess this type of noise.

References

Abramowitz, M., Stegun, I.A. (Eds.), 1972, Handbook of mathematical functions: with formulas, graphs, and mathematical tables, 10th ed., Courier Dover Publications, New York, USA.

Adams, J., Basham, P.W., 1991, The seismicity and seismotectonics of eastern Canada, in: Slemmons, D.B., Engdahl, E.R., Zoback, M.D., Blackwell, D.D. (Eds.), Neotectonics of North America, Decade Map Volume 1, Geological Society of America, Boulder, Colorado, pp. 261–276.

Agnew, D.C., 1992, The time-domain behavior of power-law noises, Geophys. Res. Lett., 19, 333–336, doi:10.1029/91GL02832.

Altamimi, Z., Collilieux, X., Métivier, L., 2011, ITRF2008: An improved solution of the international terrestrial reference frame, J Geod., 85, 457–473, doi:10.1007/s00190-011-0444-4.

Beavan, J., 2005, Noise properties of continuous GPS data from concrete pillar geodetic monuments in New Zealand and comparison with data from U.S. deep drilled braced monuments, J Geophys. Res., 110, B08410, doi:10.1029/2005JB003642.

Beran, J., 1994, Statistics for long-memory processes, Chapman and Hall/CRC Press.

Bergstrand, S., Scherneck, H.G., Lidberg, M., Johansson, J.M., 2007, BIFROST: Noise properties of GPS time series, in: Tregoning, P., Rizos, C. (Eds.), Dynamic Planet, International Association of Geodesy Symposia, Springer Berlin Heidelberg, pp. 123–130, doi:10.1007/978-3-540-49350-1_20.

Bos, M.S., Fernandes, R.M.S., Williams, S.D.P., Bastos, L., 2008, Fast error analysis of continuous GPS observations, J Geod., 82, 157–166, doi:10.1007/s00190-007-0165-x.

CRG, 2015, Centre de recherche en géomatique [WWW Document], Laval Univ., URL http://www.crg.ulaval.ca/ (accessed 1.26.15).

Dach, R., Hugentobler, U., Fridez, P., Meindl, M., 2007, The Bernese GPS software version 5.0, Astronomical Institute, University of Bern, Bern, Switzerland.

Dixon, T.H., Kornreich Wolf, S., 1990, Some tests of wet tropospheric calibration for the CASA Uno Global Positioning System experiment, Geophys. Res. Lett., 17, 203–206, doi:10.1029/GL017i003p00203.

Dmitrieva, K., Segall, P., DeMets, C., 2015, Network-based estimation of time-dependent noise in GPS position time series, J Geod., 89, 591–606, doi:10.1007/s00190-015-0801-9.

Dong, D., Fang, P., Bock, Y., Webb, F., Prawirodirdjo, L., Kedar, S., Jamason, P., 2006, Spatiotemporal filtering using principal component analysis and Karhunen-Loeve expansion approaches for regional GPS network analysis, J Geophys. Res. Solid Earth, 111, B03405, doi:10.1029/2005JB003806.

Dow, J.M., Neilan, R.E., Rizos, C., 2009, The International GNSS Service in a changing landscape of Global Navigation Satellite Systems, J Geod., 83, 191–198, doi:10.1007/s00190-008-0300-3.

Fang, X., 2013, Weighted total least squares: necessary and sufficient conditions, fixed and random parameters, J Geod., 87, 733–749, doi:10.1007/s00190-013-0643-2.

George, N.V., Tiampo, K.F., Sahu, S.S., Mazzotti, S., Mansinha, L., Panda, G., 2011, Identification of Glacial Isostatic Adjustment in Eastern Canada Using S Transform Filtering of GPS Observations, Pure Appl. Geophys., 1–11, doi:10.1007/s00024-011-0404-1.

GGE, 2014, Geodesy and Geomatics Engineering [WWW Document], Univ. New Brunswick, URL http://www2.unb.ca/gge/HomePage.php (accessed 12.18.14).

Goudarzi, M.A., Cocard, M., Santerre, R., 2015, Present-day 3D velocity field of eastern North America based on continuous GPS observations, Manuscr. Submitt. to Pure Appl. Geophys.

Goudarzi, M.A., Cocard, M., Santerre, R., Woldai, T., 2013, GPS interactive time series analysis software, GPS Solut., 17, 595–603, doi:10.1007/s10291-012-0296-2.

Henton, J.A., Craymer, M.R., Ferland, R., Dragert, H., Mazzotti, S., Forbes, D.L., 2006, Crustal motion and deformation monitoring of the Canadian landmass, Geomatica, 60, 173–191.

Hosking, J.R.M., 1981, Fractional differencing, Biometrika, 68, 165–176, doi:10.1093/biomet/68.1.165.

Johansson, J.M., Davis, J.L., Scherneck, H.G., Milne, G.A., Vermeer, M., Mitrovica, J.X., Bennett, R.A., Jonsson, B., Elgered, G., Elósegui, P., Koivula, H., Poutanen, M., Rönnäng, B.O., Shapiro, I.I., 2002, Continuous GPS measurements of postglacial adjustment in Fennoscandia 1. Geodetic results, J Geophys. Res., 107, 2157, doi:10.1029/2001JB000400.

Johnson, H.O., Agnew, D.C., 1995, Monument motion and measurements of crustal velocities, Geophys. Res. Lett., 22, 2905–2908, doi:10.1029/95GL02661.

Johnson, H.O., Wyatt, F.K., 1994, Geodetic network design for fault-mechanics studies, Manuscripta Geod., 19, 309–323.

JPL, 2014, GPS Time Series [WWW Document], Jet Propuls. Lab., Calif. Inst. Technol., URL http://sideshow.jpl.nasa.gov/post/series.html (accessed 12.19.14).

Kenyeres, A., Bruyninx, C., 2009, Noise and periodic terms in the EPN time series, in: Drewes, H. (Ed.), Geodetic Reference Frames, International Association of Geodesy Symposia, Springer Berlin Heidelberg, pp. 143–148, doi:10.1007/978-3-642-00860-3_22.

King, M.A., Williams, S.D.P., 2009, Apparent stability of GPS monumentation from short-baseline time series, J Geophys. Res. Solid Earth, 114, B10403, doi:10.1029/2009JB006319.

Klos, A., Bogusz, J., Figurski, M., Kosek, W., 2014, Uncertainties of geodetic velocities from permanent GPS observations: the Sudeten case study, Acta Geodyn. Geomater., 11, 201–209, doi:10.13168/AGG.2014.0005.

Lambert, A., Courtier, N., Sasagawa, G., Klopping, F., Winester, D., James, T.S., Liard, J.O., 2001, New constraints on Laurentide postglacial rebound from absolute gravity measurements, Geophys. Res. Lett., 28, 2109, doi:10.1029/2000GL012611.

Langbein, J., 2008, Noise in GPS displacement measurements from Southern California and Southern Nevada, J Geophys. Res., 113, B05405, doi:10.1029/2007JB005247.

Langbein, J., 2004, Noise in two-color electronic distance meter measurements revisited, J Geophys. Res., 109, B04406, doi:10.1029/2003JB002819.

Langbein, J., Johnson, H., 1997, Correlated errors in geodetic time series: Implications for time-dependent deformation, J Geophys. Res. Solid Earth, 102, 591–603.

Langbein, J., Wyatt, F., Johnson, H., Hamann, D., Zimmer, P., 1995, Improved stability of a deeply anchored geodetic monument for deformation monitoring, Geophys. Res. Lett., 22, 3533–3536.

Lavoie, C., Allard, M., Duhamel, D., 2012, Deglaciation landforms and C-14 chronology of the Lac Guillaume-Delisle area, eastern Hudson Bay: A report on field evidence, Geomorphology, 159-160, 142–155, doi:10.1016/j.geomorph.2012.03.015.

Lidberg, M., Johansson, J.M., Scherneck, H.G., Milne, G.A., 2010, Recent results based on continuous GPS observations of the GIA process in Fennoscandia from BIFROST, J Geodyn., 50, 8–18, doi:10.1016/j.jog.2009.11.010.

Mandelbrot, B.B., 1977, Fractals: form, chance and dimension, Freeman, San Francisco, CA.

Mandelbrot, B.B., Van Ness, J.W., 1968, Fractional Brownian motions, fractional noises and applications, SIAM Rev., 10, 422–437.

Mao, A., Harrison, C.G.A., Dixon, T.H., 1999, Noise in GPS coordinate time series, J Geophys. Res., 104, 2797–2816, doi:10.1029/1998JB900033.

Mazzotti, S., James, T.S., Henton, J.A., Adams, J., 2005, GPS crustal strain, postglacial rebound, and seismic hazard in eastern North America: The Saint Lawrence valley example, J Geophys. Res., 110, B11301, doi:10.1029/2004JB003590.

MERNQ, 2014, Geodetics and GPS Technology [WWW Document], Minist. Energy Nat. Resour. Quebec, URL http://www.mern.gouv.qc.ca/english/territory/expertise/expertise-geodetics.jsp (accessed 12.17.14).

Mikhail, E.M., Ackermann, F.E., 1976, Observations and least squares, IEP, New York, USA.

Montillet, J.P., Tregoning, P., McClusky, S., Yu, K., 2013, Extracting white noise statistics in GPS coordinate time series, IEEE Geosci. Remote Sens. Lett., 10, 563–567.

NGS, 2014a, Continuously Operating Reference Station (CORS) [WWW Document], Am. Natl. Geod. Surv, URL http://geodesy.noaa.gov/CORS/ (accessed 12.17.14).

NGS, 2014b, National Geodetic Survey [WWW Document], Natl. Ocean Atmos. Adm, URL http://www.ngs.noaa.gov/ (accessed 12.19.14).

Nikolaidis, R.M., 2002, Observation of geodetic and seismic deformation with the Global Positioning System (Ph.D. Thesis), University of California, San Diego, San Diego.

Nistor, S., Buda, A.S., 2014, Velocity component analysis on a GNSS network, RevCAD J Geod. Cadastre, 17, 52–59.

NRCan, 2014, Canadian Active Control System [WWW Document], Nat. Resour. Canada, URL http://www.nrcan.gc.ca/earth-sciences/geomatics/geodetic-reference-systems/tools-applications/rinex-observations-files/9092 (accessed 12.17.14).

Park, K.D., Nerem, R.S., Davis, J.L., Schenewerk, M.S., Milne, G.A., Mitrovica, J.X., 2002, Investigation of glacial isostatic adjustment in the northeast US using GPS measurements, Geophys. Res. Lett., 29, 1509, doi:10.1029/2001GL013782.

Penna, N.T., Stewart, M.P., 2003, Aliased tidal signatures in continuous GPS height time series, Geophys. Res. Lett., 30, 2184, doi:10.1029/2003GL018828.

Press, W.H., Teukolsky, S.A., Vetterling, W.T., Flannery, B.P., 1992, Numerical Recipes in C: The Art of Scientific Computing, 2nd ed., Cambridge University Press, New York, USA.

QGIS, D.T., 2015, QGIS Geographic Information System. Open Source Geospatial Foundation Project, http://qgis.osgeo.org (accessed 12.19.14).

Rice, J., 2006, Mathematical statistics and data analysis, 3rd ed., Duxbury Press.

Scargle, J.D., 1989. Studies in astronomical time series analysis. III-Fourier transforms, autocorrelation functions, and cross-correlation functions of unevenly spaced data, Astrophys. J, 343, 874–887.

Scargle, J.D., 1982, Studies in astronomical time series analysis. II-Statistical aspects of spectral analysis of unevenly spaced data, Astrophys. J, 263, 835–853.

Scargle, J.D., 1981, Studies in astronomical time series analysis. I-Modeling random processes in the time domain, Astrophys. J, Suppl. Ser., 45, 1–71.

SCG, 2014, Department of Geomatics Sciences [WWW Document], Laval Univ., URL http://www.scg.ulaval.ca/index.php (accessed 12.19.14).

Schaffrin, B., Wieser, A., 2008, On weighted total least-squares adjustment for linear regression, J Geod., 82, 415–421, doi:10.1007/s00190-007-0190-9.

Schulz, M., Stattegger, K., 1997, SPECTRUM: Spectral analysis of unevenly spaced paleoclimatic time series, Comput. Geosci., 23, 929–945.

Sella, G.F., Stein, S., Wdowinski, S., Dixon, T.H., Craymer, M.R., James, T.S., 2004, Direct constraints on GIA motion in North America using GPS, in: AGU Spring Meeting Abstracts, p. 3.

Sigrist, P., Coppin, P., Hermy, M., 1999, Impact of forest canopy on quality and accuracy of GPS measurements, Int. J Remote Sens., 20, 3595–3610, doi:10.1080/014311699211228.

Strang, G., Borre, K., 1997, Linear algebra, geodesy, and GPS, Wellesley Cambridge Press.

Teferle, F.N., Williams, S.D.P., Kierulf, H.P., Bingley, R.M., Plag, H.P., 2008, A continuous GPS coordinate time series analysis strategy for high-accuracy vertical land movements, Phys. Chem. Earth, 33, 205–216, doi:10.1016/j.pce.2006.11.002.

Tiampo, K.F., Mazzotti, S., James, T.S., 2012, Analysis of GPS Measurements in Eastern Canada Using Principal Component Analysis, Pure Appl. Geophys., 169, 1483–1506, doi:10.1007/s00024-011-0420-1.

Tiampo, K.F., Rundle, J.B., Klein, W., Ben-Zion, Y., McGinnis, S., 2004, Using eigenpattern analysis to constrain seasonal signals in Southern California, Pure Appl. Geophys., 161, 1991–2003, doi:10.1007/s00024-004-2545-y.

Trauth, M.H., 2010, MATLAB recipes for Earth Sciences, 3rd ed., Springer.

Wdowinski, S., Bock, Y., Zhang, J., Fang, P., Genrich, J., 1997, Southern California Permanent GPS Geodetic Array: Spatial filtering of daily positions for estimating coseismic and postseismic displacements induced by the 1992 Landers earthquake, J Geophys. Res., 102, 18057–18070.

Williams, S.D.P., 2008, CATS: GPS coordinate time series analysis software, GPS Solut., 12, 147–153.

Williams, S.D.P., 2003, The effect of coloured noise on the uncertainties of rates estimated from geodetic time series, J Geod., 76, 483–494, doi:10.1007/s00190-002-0283-4.

Williams, S.D.P., Bock, Y., Fang, P., Jamason, P., Nikolaidis, R.M., Prawirodirdjo, L., Miller, M., Johnson, D.J., 2004, Error analysis of continuous GPS position time series, J Geophys. Res., 109, B03412, doi:10.1029/2003JB002741.

Williams, S.D.P., Willis, P., 2006, Error analysis of weekly station coordinates in the DORIS network, J Geod., 80, 525–539, doi:10.1007/s00190-006-0056-6.

Xu, G., 2007, GPS: theory, algorithms, and applications, 2nd ed., Springer Verlag.

Zhang, J., Bock, Y., Johnson, H., Fang, P., Williams, S.D.P., Genrich, J., Wdowinski, S., Behr, J., 1997, Southern California Permanent GPS Geodetic Array: Error analysis of daily position estimates and site velocities, J Geophys. Res. Solid Earth, 102, 18035–18055.
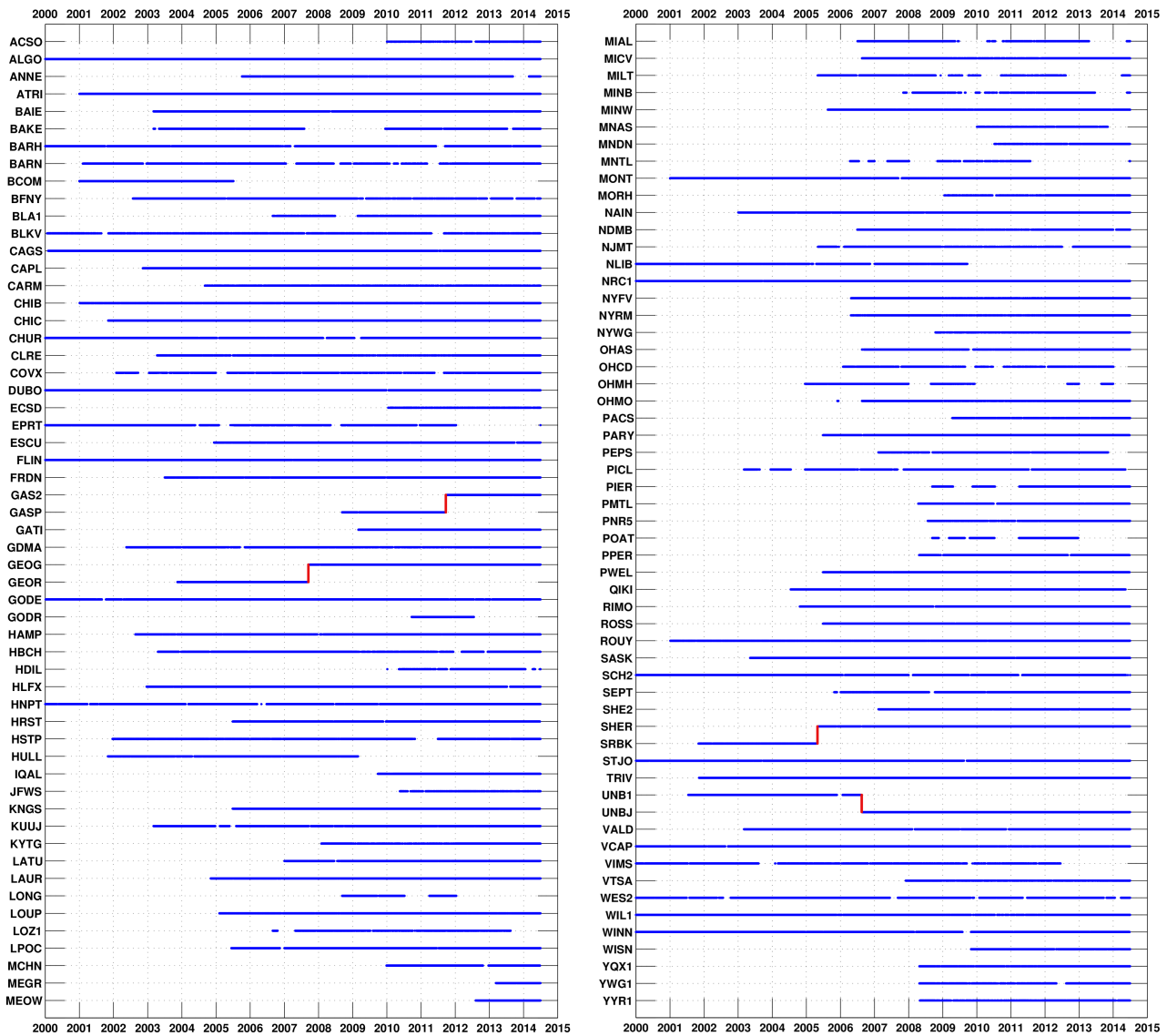
Appendix

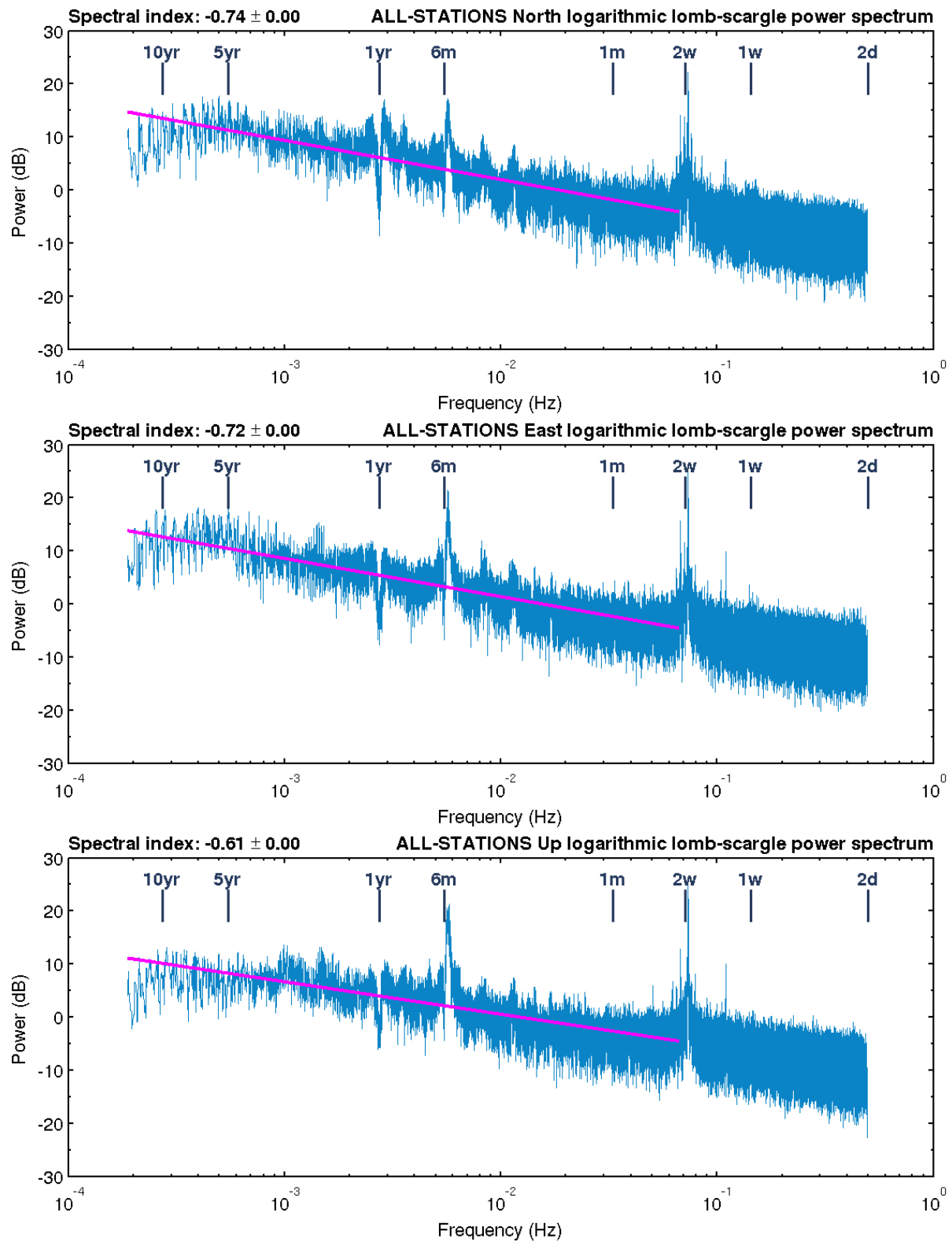**Figure A.1:** Data map of CGPS observations.

Figure A.2: The common power spectrum for all CGPS stations filtered with the window length of 11 days.
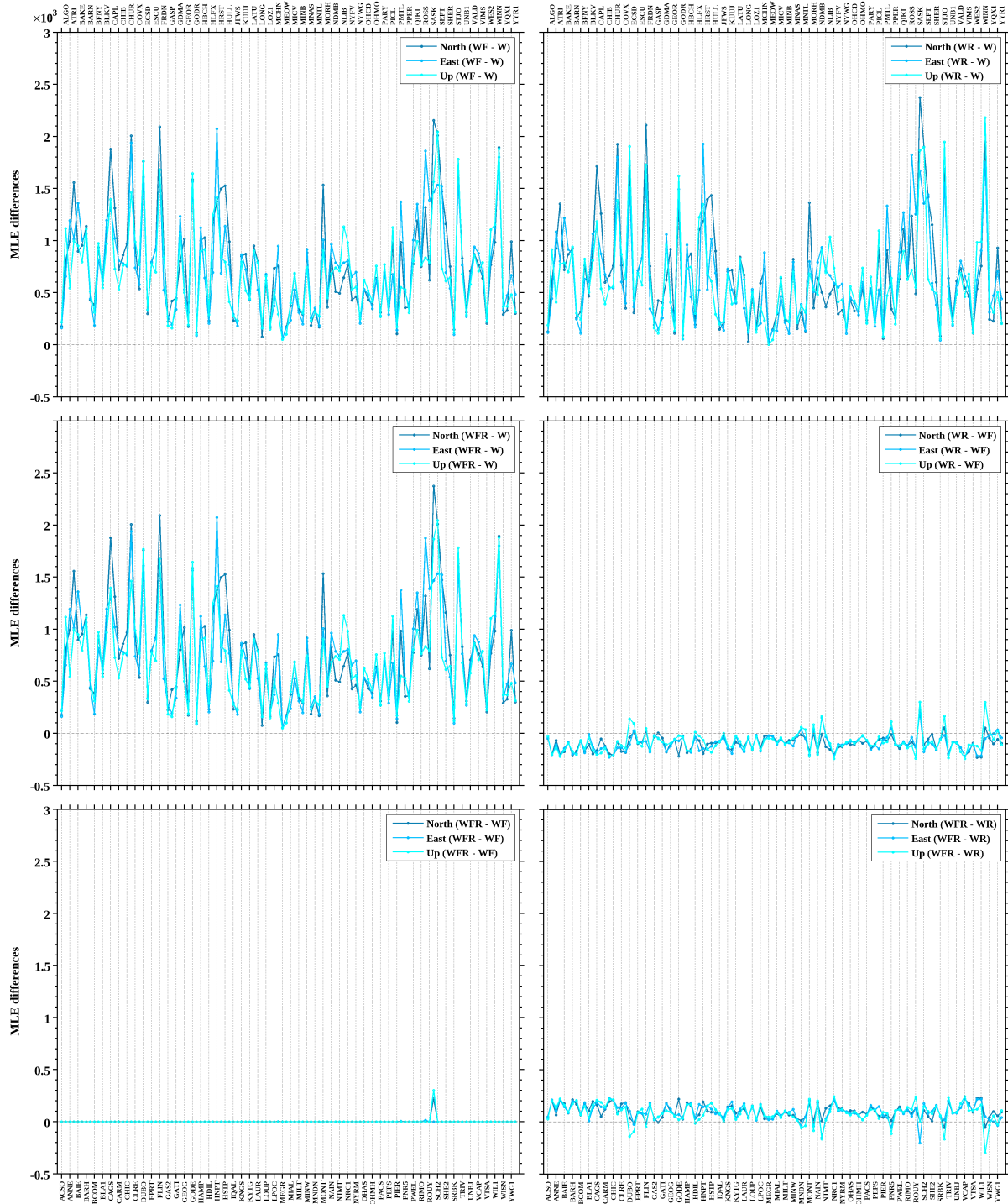
Figure A.3: Comparison of different noise models according to the Maximum Likelihood Estimation values.